

Matti Aula

OPTICAL EMISSION FROM ELECTRIC ARC FURNACES

UNIVERSITY OF OULU GRADUATE SCHOOL;
UNIVERSITY OF OULU, FACULTY OF TECHNOLOGY



ACTA UNIVERSITATIS OULUENSIS
C Technica 558

MATTI AULA

**OPTICAL EMISSION FROM ELECTRIC
ARC FURNACES**

Academic dissertation to be presented, with the assent of the Doctoral Training Committee of Technology and Natural Sciences of the University of Oulu, for public defence in the Wetteri auditorium (IT115), Linnanmaa, on 29 January 2016, at 12 noon

UNIVERSITY OF OULU, OULU 2016

Copyright © 2016
Acta Univ. Oul. C 558, 2016

Supervised by
Professor Timo Fabritius
Professor Marko Huttula

Reviewed by
Associate Professor Anders Tilliander
Doctor Valentina Colla

Opponent
Professor Chris Pistorius

ISBN 978-952-62-1091-9 (Paperback)
ISBN 978-952-62-1092-6 (PDF)

ISSN 0355-3213 (Printed)
ISSN 1796-2226 (Online)

Cover Design
Raimo Ahonen

JUVENES PRINT
TAMPERE 2016

Aula, Matti, Optical emission from electric arc furnaces.

University of Oulu Graduate School; University of Oulu, Faculty of Technology

Acta Univ. Oul. C 558, 2016

University of Oulu, P.O. Box 8000, FI-90014 University of Oulu, Finland

Abstract

The main cause of temperature and composition fluctuations in the electric arc furnace (EAF) process is the scrap used as a raw material. Process conditions in EAF can vary significantly from heat to heat because there is no accurate information of scrap composition. Due to harsh process conditions, there are currently few sensors available for direct on-line measurement of the EAF process.

In this work new information about stainless steelmaking EAF process conditions is sought with optical emission spectrum measurement. The measurement system relies on transportation of the light emitted from the measured furnace to a remotely situated spectrometer.

Analysing the slag composition from the arc emission spectrum was tested in the laboratory and on a pilot scale. The laboratory measurements indicate that the composition ratios including CrO_x or MnO have the highest correlations to the XRF analysed slag composition. The pilot scale measurements show that the Cr_2O_3 content of the slag can be measured from the arc emission spectrum using suitable reference lines with an average absolute error of 0.62 %-points and a standard deviation of 0.49 %-points.

The results from measurements at Outokumpu Stainless Oy, Tornio Works, indicate that measurement of the optical emission spectrum from industrial EAF is feasible in a practical sense, and can be used in analysing of EAF atmosphere, scrap melting and slag surface. Furthermore, the results of industrial measurements indicate that the atoms in the arc plasma mainly originate from the slag. The measurement of scrap melting could be potentially used in EAF control in optimization of arc voltages and second scrap bucket charging. The potential use of slag CrO_x measurements is in optimization of reductant additions as well as defining the further processing of EAF slag.

Keywords: EAF, in situ, measurement, OES, on-line, plasma diagnostics, process conditions, slag composition

Aula, Matti, Valokaariuunien optinen emissiospektri.

Oulun yliopiston tutkijakoulu; Oulun yliopisto, Teknillinen tiedekunta

Acta Univ. Oul. C 558, 2016

Oulun yliopisto, PL 8000, 90014 Oulun yliopisto

Tiivistelmä

Valokaariuunien ohjaus on perinteisesti ollut uunioperaattorin käsissä. Valokaariuuniprosessin on-line mittaukseen on olevassa vähän menetelmiä johtuen uunin hyvin haastavaista olosuhteista.

Tässä työssä on tutkittu optiseen emissiospektroskopiaan perustuvaa menetelmää uuden jatkuva-aikaisen tiedon tuottamisessa valokaariuuniprosessista. Mittausjärjestelmä perustuu valon keräämiseen mitattavasta uunista valokuidun avulla, joka johtaa valon analysoitavaksi etäälle prosessista sijoitettuun spektrometriin. Mittauksia suoritettiin laboratorio-, pilot- ja tehdasmittakaavassa.

Valokaariuunin kuonan koostumuksen analysointia testattiin laboratorio- ja pilot-mittakaavauuneilla. Laboratoriomittaukset osoittivat että koostumussuhteilla, joissa oli mukana CrO_x tai MnO , oli suurin korrelaatio kuonan XRF-analyysillä mitattuun koostumukseen. Pilot-mittakaavan kokeissa havaittiin, että kuonan Cr_2O_3 -pitoisuutta voidaan mitata valokaaren emissiospektristä 0,62 %-yksikön keskimääräisellä absoluuttisella virheellä ja 0,49 %-yksikön keskihajonnalla.

Teollisella valokaariuunilla suoritetuista mittauksista havaittiin, että optisen emissiospektrin mittaus voidaan suorittaa ilman ylitsepääsemättömiä teknisiä esteitä. Mittauksen tuloksia voidaan puolestaan käyttää kaasufaasin reaktioiden, romun sulamisen ja kuonapinnan ominaisuuksien arvioinnissa. Valokaaren emissiospektrin analyysi osoitti, että valokaaren plasman komponentit ovat pääosin peräisin kuonasta, joka mahdollistaa kuonan koostumuksen arvioinnin valokaaren emissiospektrin perusteella. Romun sulamisen mittausta voidaan prosessinohjauksessa käyttää jänniteportaiden ja toisen korin panostuksen optimointiin. Kuonan kromipitoisuuden mittaamista voidaan puolestaan käyttää pelkistinaineiden lisäyksen optimointiin ja kuonan jatkokäsittelyn valintaan.

Asiasanat: EAF, in situ, kuonan koostumus, mittaus, OES, on-line, plasmadiagnostiikka, prosessiolosuhteet

Acknowledgements

This dissertation was completed in the course of approximately four years in 2011 – 2015. The early part of my research was funded by Finnish Funding Agency for Technology and innovation (Tekes) TULI and TUTLI programs, which emphasize the commercialization of the studied methods. The crucial phase of reporting the findings and finishing the dissertation was funded by Technology Industries of Finland Centennial Foundation Fund for the Association of Finnish Steel and Metal Producers. System Integrated Metals Processing (SIMP) research program coordinated by Finnish Metals and Engineering Competence Cluster (FIMECC), Emil Aaltonen Foundation and University of Oulu Graduate School (UniOGS) are also acknowledged for financial support.

Many people from University of Oulu have helped me during these years. I want thank my supervisors Prof. Timo Fabritius and Prof. Marko Huttula for guidance and support. I want to express my gratitude to Prof. Timo Fabritius for giving me a chance to work in field of process metallurgy and trusting me with this interesting topic. Dr. Ari Mäkinen from Optoelectronics Group is acknowledged for passing me the baton and providing support on plasma physics. Mr. Juha Roininen is acknowledged for support in important early periods of research. Associate Professor Anders Tilliander and Dr. Valentina Colla are acknowledged for being pre-examiners of this work and providing constructive feedback on the dissertation.

My colleagues at Process Metallurgy Group have provided a working atmosphere both relaxing and encouraging. If a certain distinction has to be made, the people who I owe most are: Mr. Ville-Valtteri Visuri, Mr. Mikko Iljana, Mr. Tuomas Alatarvas, Mr. Olli Peltosaari and Dr. Eetu-Pekka Heikkinen. In addition, the inspiration and refreshing views provided by our lunch club, the Fab five and Hulk, should not be underestimated.

I would like to thank people in Outokumpu Stainless, Tornio Works, for giving me the chance to develop this measurement system at their EAF and giving me invaluable advice from practical perspective. I want to specifically thank Mr. Kimmo Vallo from Steel melt shop, as well as Mr. Juho Kunelius and Dr. Paavo Hooli from Tornio Research Center. Mr. Sauli Pisilä and Mr. Lauri Närhi from Outotec, as well as Mr. Ville Fomkin and Mrs. Helena Erkkilä from Ovako Steel Imatra are acknowledged for providing me a chance to conduct measurements in their electric arc furnaces.

In spring 2014 I had a chance to visit Aachen RWTH University, Department of Industrial Furnaces and Heat Engineering (IOB). I want to thank Mr. Thorsten Demus, Dr. Thomas Echterhof, Prof. Herbert Pfeifer and whole staff of IOB for fruitful co-operation and giving me a glimpse how the research is conducted in Germany.

During these four years, I have witnessed the foundation of Luxmet Oy. I want to thank Mr. Ahti Leppänen, Mr. Mikko Jokinen and Mr. Tommi Sallinen for giving me a chance to build something commercially relevant together. Without the work by Mr. Ahti Leppänen on the spectrum analysis software, this dissertation would have taken much longer time.

Last but not the least, I want to thank my relatives and family for supporting my PhD endeavour. I want to thank my father Jukka and mother Auli, whose importance cannot be described by words. My last acknowledgements go to my brothers Kari and Ville, who have always encouraged me and share my scientific aspirations.

Oulu, December 2015

Matti Aula

List of abbreviations and symbols

EAF	Electric arc furnace
OES	Optical emission spectrometry
LTE	Local thermodynamic equilibrium
AC	Alternating current
DC	Direct current
VOC	Volatile organic compound
PC	Post-combustion
CCD	Charge-coupled device
XRF	X-ray fluorescence
UV	Ultra-violet
VIS	Visible
FWHM	Full width at half maximum
MS	Mass spectrometry
CrO _x	Chromium oxide of undefined oxidation state
N^Z	Number density
g_j	Degeneracy of the upper level
E_j^z	Energy of the upper level
$U^z(T)$	Partition function
k	Boltzmann constant
ε_{ij}^z	Intensity of the emission line
A_{ij}	Transition probability
λ	Wavelength
h	Planck's constant
c	Speed of light
M	Photon flux
T	Temperature
R	Intensity ratio
τ	Optical depth

List of original publications

This thesis is based on the following publications, which are referred to throughout the text by their Roman numerals:

- I Aula M, Mäkinen A, Fabritius T (2013) Analysis of arc emission spectra of stainless steel electric arc furnace slag affected by fluctuating arc voltage. *Applied Spectroscopy*. 68(1): 26–32.
- II Aula M, Demus T, Echterhof T, Huttula M, Pfeifer H, Fabritius T (2015) On-line Analysis of Cr₂O₃ content of the slag in pilot scale EAF by measuring the optical emission spectrum of the electric arc. [Manuscript].
- III Aula M, Leppänen A, Roininen J, Heikkinen E.-P, Vallo K, Fabritius T and Huttula M (2014) Characterization of Process Conditions in Industrial Stainless Steelmaking Electric Arc Furnace Using Optical Emission Spectrum Measurements. *Metallurgical and Materials Transactions B*. 45B(6): 839–849.
- IV Aula M, Mäkinen A, Leppänen A, Huttula M, Fabritius T (2015) Optical emission analysis of slag surface conditions and furnace atmosphere during different process stages in electric arc furnace (EAF). *ISIJ International*. 55(8): 1702–170.

The author of this dissertation was mainly responsible for all of the publications listed above. The experimental tests reported in the publications were conducted collaboratively between the author and co-authors. The author was responsible for analysing the measurement results obtained from the laboratory, pilot and industrial tests.

Other related publications by author:

- Aula M, Fabritius T, Fomkin V (2015) Measurement of Hot-spot Optical Emission Spectrum from Industrial Electric Arc Furnace Used in Making of Carbon Steel. *Proceedings of the 6th International Congress on the Science and Technology of Steelmaking*. The Chinese Society for Metals. Beijing, China
- Aula M, Fabritius T, Pisilä S (2015) On-line analysis of process conditions in ilmenite smelting with optical emission spectrometry. *Proceedings of EMC 2015*. GDMB Verlag GmbH. Düsseldorf. Germany
- Pisilä S, Palovaara P, de Jong A, Aula M (2015) Ilmenite Smelting in a Pilot Scale DC Furnace. *Proceeding of the Fourteenth International Ferroalloys Congress*. Kiev. Ukraine.

Table of contents

Abstract	
Tiivistelmä	
Acknowledgements	7
List of abbreviations and symbols	9
List of original publications	11
Table of contents	13
1 Introduction	15
1.1 Context – Electric arc furnace steelmaking.....	15
1.2 Objectives and scope.....	15
2 Methods	17
2.1 Optical emission spectrum.....	17
2.1.1 Atomic and ionic emissions.....	17
2.1.2 Thermal radiation.....	18
2.2 Optical emission spectrometry.....	18
2.3 Plasma diagnostics of LTE plasma.....	19
2.3.1 Plasma temperature in LTE plasma.....	20
3 Electric arc furnace steelmaking	21
3.1 Electric arc furnace.....	21
3.2 Main process periods in EAF steelmaking.....	22
3.3 EAF auxiliary equipment.....	25
3.4 Stainless steelmaking EAF.....	26
3.5 On-line data of EAF.....	26
4 Optical conditions inside industrial EAFs	31
4.1 Gas composition of EAF atmosphere.....	31
4.2 EAF Dust.....	32
4.2.1 Dust generation.....	33
4.2.2 Optical thickness of EAF atmosphere.....	34
4.2.3 Significance of optical thickness in optical measurements.....	36
4.3 EAF arc plasma.....	37
4.3.1 Validity of LTE assumption in industrial furnaces.....	38
4.3.2 Plasma temperature.....	38
4.3.3 Optical thickness of arc plasma.....	39
4.3.4 Modelling heat transfer from arc plasma.....	40
5 Experiments	43
5.1 Laboratory furnace.....	43

5.1.1	Measurement equipment.....	44
5.1.2	EAF slag samples	44
5.1.3	Correction of spectral data.....	46
5.2	Pilot-scale EAF	47
5.2.1	Furnace description.....	47
5.2.2	Measurement system description.....	47
5.2.3	Test period description.....	48
5.2.4	Data handling.....	49
5.3	Industrial EAF	49
5.3.1	Measurement system	51
5.3.2	Emission spectrum analysis.....	54
6	Results and discussion	57
6.1	Characteristics of EAF arc plasma	58
6.2	EAF slag composition	61
6.2.1	Feasibility of analysing slag composition ratios with fluctuating arc length.....	61
6.2.2	Accuracy of analysing slag CrO _x content	62
6.3	EAF process conditions.....	64
6.3.1	Volatilization of scrap contaminants.....	66
6.3.2	Spontaneous generation of CO	67
6.3.3	Scrap melting.....	68
6.3.4	Slag surface conditions.....	69
7	Industrial relevance	71
7.1	Slag composition calculated from arc emission spectrum	71
7.2	Average scrap melting.....	72
7.3	Optimization of arc voltage.....	73
7.4	Assumptions of EAF heat transfer models.....	74
7.5	Implications for the development in the future	74
8	Summary	75
	References	77
	Original publications	83

1 Introduction

1.1 Context – Electric arc furnace steelmaking

Steel scrap is used as a raw material in electrical steelmaking. The scrap inserted into an electric arc furnace (EAF) is melted with electricity. The electricity is supplied via the electrodes to the scrap charge. Finally the liquid steel is tapped out for further processing.

The most challenging aspect of EAF steelmaking is the varying attributes of the steel scrap. The density, size and composition of scrap all vary depending on where the scrap originates from and how the scrap has been separated. Different types of steel scrap are separated into different categories, but to know exactly what the scrap contains would mean there would have to be as many scrap categories should be employed as there are sources of scrap. No scrap supplier uses this tedious classification practice. The consequence is that a certain scrap category always contains scrap pieces of different origins and the characteristics of the EAF charge vary.

1.2 Objectives and scope

Recently, the focus in EAF development has been switched towards dynamic control, which gives the operator new possibilities to monitor and adjust the EAF process during the heat [1]. On the other hand, there are too few sensors that can withstand the harsh process conditions of EAF. The lack of on-line data combined with no accurate information of scrap composition cause significant variance in tapping temperature, metal yield and energy efficiency, which are in the worst case only observed after the tapping.

The aim of this thesis is to introduce a new method for analysing EAF process conditions based on on-line *in situ* optical emission spectrometry and to report its advantages and limitations. The focus of this thesis is in stainless steelmaking because poor process control in EAF can cause losses of valuable elements like Ni and Cr, and the fluctuation in the content of other elements in scrap can have a significant effect on the process phenomena.

The original papers and their relations to the analysed phenomena and to the scale of the measurements are presented in Table 1. The original publications in this thesis are ordered based on the scale of the furnace from which the optical

emission spectra were measured. Measurements were conducted in a laboratory furnace (Paper I), in a pilot EAF (Paper II) and in an industrial furnace (Papers III and IV).

The three main topics of the original papers were characteristics of EAF plasma, EAF slag composition and EAF process conditions. The characteristics of EAF plasma were analysed to provide better understanding of composition and optical thickness of EAF arc plasma, which can be used to make better assumptions in plasma modelling. EAF slag composition was analysed because it affects slag foaming and chromium losses in stainless steelmaking EAF. The aim of measuring EAF process conditions was to provide new dynamic information about scrap melting, post combustion in EAF atmosphere and heat transfer between the roof and the slag surface.

This dissertation consists of a description of methods, an introduction to EAF steelmaking and optical characteristics of EAF, a description of the experiments reported in the original papers, a summary of results obtained from the measurements and a discussion about the industrial relevance of the findings. The original papers are reprinted at the end of this dissertation.

Table 1. Original papers and their relation to the analysed phenomena and to the scale of the measurements.

Scale	Characteristics of EAF arc plasma	EAF slag composition	EAF process conditions
Laboratory	Paper I	Paper I	<i>Not applicable</i>
Pilot	Paper II	Paper II	Paper II
Industrial	Paper III	<i>In future</i>	Papers III and IV

2 Methods

2.1 Optical emission spectrum

Emission spectrum describes the intensity of electromagnetic radiation as a function of wavelength. The term “optical” refers to electromagnetic radiation of wavelengths visible to the human eye. Many different mechanisms produce electromagnetic radiation, but in the context of the electric arc furnace and visible wavelengths, the two main mechanisms are atomic or ionic emissions and thermal motion of particles.

2.1.1 Atomic and ionic emissions

Atomic and ionic emissions are caused by the movement of electrons between different energy states. The schematic illustration of atomic emission is presented in Figure 1. Atomic emission is preceded by the movement of electron to higher energy levels due to the absorption of energy (while still being bound). When the electron returns to lower energy levels, electromagnetic radiation is emitted. The wavelength of the radiation is proportional to the difference between the two energy levels, which means that since orbital configurations of all atoms are unique, so are the wavelengths of atomic emissions. The wavelengths of the atomic emissions are generally in the visible spectrum, while the ionic emissions are generally in lower wavelengths.

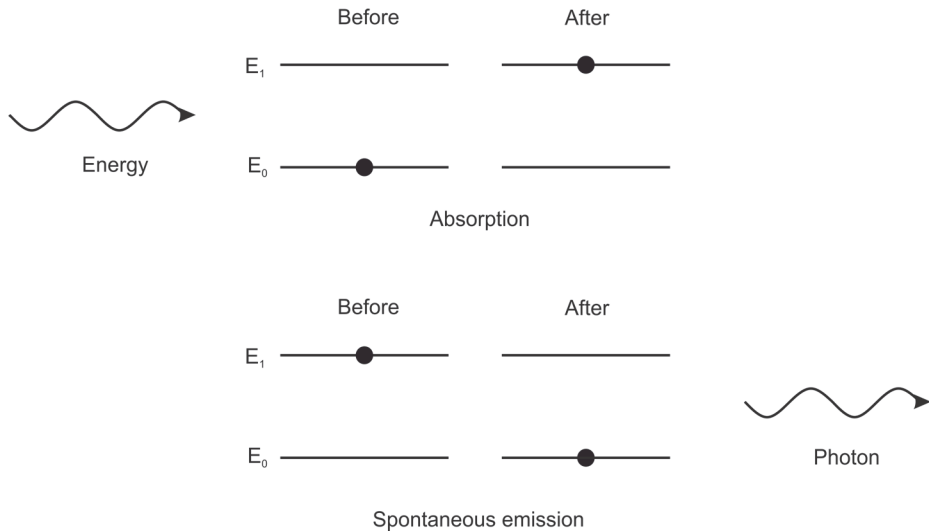


Fig. 1. Subsequent absorption and spontaneous emission.

2.1.2 Thermal radiation

Thermal radiation is electromagnetic radiation arising as a result of microscopic thermal activities in a material approximately in local equilibrium [2]. The thermal radiation emitted by the material contains photons of multiple wavelengths; in black body conditions the intensity of the thermal radiation depends only on the temperature of the material. In practice, the surface properties affect the intensity of the emitted radiation. The ratio of the emitted radiation of a certain wavelength to black body radiation can be expressed by emissivity. The thermal radiation can be simplified with grey body assumption, which assumes that the emissivity is constant in all wavelengths, i.e. the wavelength distribution of the thermal radiation is equivalent to that of black body radiation. In steelmaking, liquid steel and slag are often assumed to emit thermal radiation as a grey body. The difference between the liquid steel and slag surface is that slag has much higher emissivity.

2.2 Optical emission spectrometry

Using electricity to generate atomic excitation is one of the oldest material characterization methods based on optical emission spectrometry (OES). The amount of analysed element is calculated from the ratio of atomic emission lines.

The atomic emission lines of the analysed components are compared to the atomic emission lines of the reference component, of which the amount in the material is known. The comparison of atomic emission lines makes the measurement free of the changes in overall intensity levels of the spectrum.

The use of OES in the measurement of industrial processes can be regarded as on-line OES, to separate it from traditional laboratory OES analysis. The on-line OES differs from analytic OES in the sense that it needs to be more robust to changes in excitation conditions because the economics of the process define the energy input. This means that the accuracy of on-line OES is inherently lower than analytic OES.

On-line OES has been employed in control of processes employing lasers or thermal plasma. With on-line OES it is possible to measure and correct deviations from the optimal laser welding parameters [3]. On-line OES has been used for control purposes, for example, in plasma spraying process [4], metal deposition process [5].

In steelmaking, the attempts to use on-line OES have been focused on the converter process. It has been used in analysing particle temperature and optical thickness of the EAF off-gas [6], as well as in the measurement of steel manganese content from the lance hot-spot [7]. In electric arc furnace steelmaking, two different optical emission spectrum measurements have been reported: in pilot scale ilmenite smelting [8] and in industrial DC EAF [9].

2.3 Plasma diagnostics of LTE plasma

To understand the effect of changing excitation conditions, the characteristics of the emitting material have to be defined. Fluctuation excitation conditions change the relative excitation probabilities of atoms, since the excitation levels of all atoms are unique. These changes can be modelled when the characteristics of the emitting material are well known.

The normal definition of temperature describing the thermal movement of particles is not valid in plasma because a major part of the energy is transferred through collisions of electrons. Therefore, a better description of the energetic qualities of plasma is obtained by measuring the density and temperature of the electrons. The electron temperature is often called plasma temperature, which should not be confused with particle temperature.

Most methods of plasma diagnostics rely on the plasma being in local thermodynamic equilibrium (LTE). There are many definitions of LTE, but the

general principle is that the collisional processes dominate the heat transfer in plasma. If the radiative processes are dominant, the intensity source function is no longer function of local electron temperature but depends on the radiative flux from the other parts of plasma [10].

Another assumption that can be made in plasma diagnostics is to assume the low optical thickness of plasma. In optically thick conditions, the spectral lines are affected by absorption of the cooler outer region of plasma. Most widely used methods for determination of plasma parameters rely on optically thin spectral lines [11].

2.3.1 Plasma temperature in LTE plasma

In LTE plasma the population densities of excited energy levels and electron temperature T is related through the Boltzmann function:

$$\frac{N_j^z}{N^z} = \frac{g_j e^{-\frac{E_j^z}{kT}}}{U^z(T)} \quad (1)$$

where N^z is the number density, g_j is the degeneracy of the upper level, E_j^z is the energy of the upper level, $U^z(T)$ is the partition function and k is the Boltzmann constant [12]. The consequence of the Boltzmann function is that the wavelength-integrated emissivity \mathcal{E}_{ij}^z , for a transition of a given emitting species, can be expressed as:

$$\ln\left(\frac{\mathcal{E}_{ij}^z \lambda}{A_{ij} g_j}\right) = -\frac{1}{kT} E_j^z + \ln\left(\frac{hcN^z}{4\pi U^z(T)}\right) \quad (2)$$

where A_{ij} is the transition probability, λ is the transition wavelength, h is the Planck's constant, c is the speed of light [13]. When the left hand side of the equation is plotted against excitation energy for all selected atomic emission lines of a single emitting species, a straight line yielding plasma temperature as its slope is expected. The term in the far right in the equation can be neglected because it is constant at a fixed plasma temperature. This method, in which electron temperature is calculated from relative line strengths, is called the Boltzmann plot method.

3 Electric arc furnace steelmaking

3.1 Electric arc furnace

EAFs generally consist of a furnace mantle, refractory lining, an off-gas duct, electrodes and an electrode arm. The energy is supplied to the electrodes via electrode arms from the EAF transformer, which is located nearby the furnace. A schematic picture of EAF is presented in Figure 2.

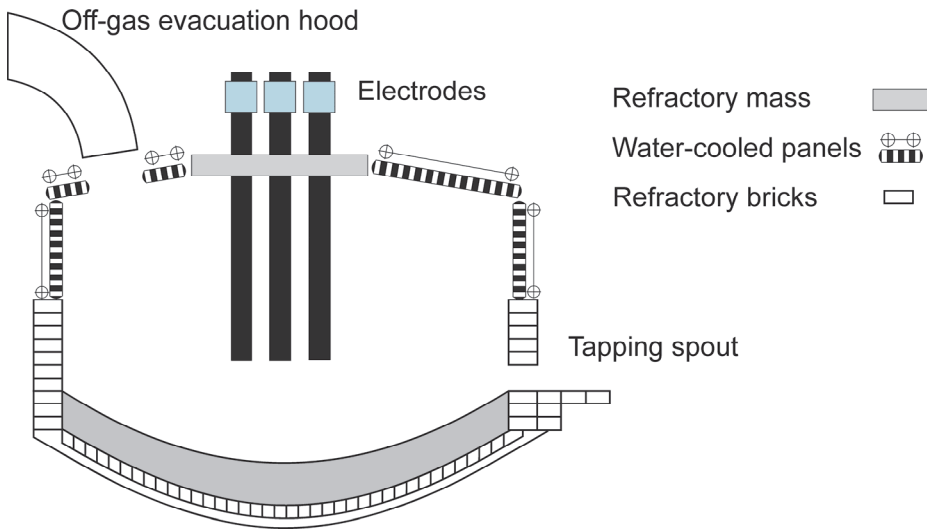


Fig. 2. Schematic picture of EAF (furnace shell omitted, modified from [14]).

The EAF mantle gives an EAF its shape. The next layer inside the mantle is the water-cooled panels, which ensure the mantle withstands the high temperatures of the EAF process. The furnace bottom and lower part of the furnace sides are protected with a ceramic lining, for example, carbon-magnesia bricks or refractory mass. The lining prevents direct contact between the liquid steel and the furnace mantle. The upper side of the EAF and furnace roof do not generally have refractory lining, but water-cooled panels are coated by an autogenous slag lining, which is generated by the splashing of the slag on the water cooled panels. In the centre of the EAF roof, around the electrodes, is a ceramic lining that insulates the electrodes from each other and the furnace mantle.

The electrical furnaces can be divided into two main categories: alternate current (AC) and direct current (DC) furnaces. AC furnaces differ from DC furnaces in current supply and in distribution of current inside the furnace. In AC furnaces, the current flows between the electrodes on the top of the steel melt, while in DC furnaces the current flows from the electrode on top of the melt to the electrode on the bottom of the furnace.

3.2 Main process periods in EAF steelmaking

The EAF process can be divided to four main process periods: 1. Charging period 2. Melting periods 3. Heating period and 4. Tapping period. Electricity is introduced to EAF in melting and heating periods, while charging and tapping periods are related to the movement of metal to and from the EAF.

The EAF process starts with the loading of scrap into the EAF. The loading is conducted with a scrap bucket, which is emptied into the EAF. The scrap bucket also contains slag formers and other additions to the furnace. The scrap can be preheated to remove the excess moisture from the scrap, which poses a safety risk in EAF processing.

After the scrap is loaded, the electrodes are lowered into the scrap and the arc is initiated. A schematic figure of scrap melting in diametrical furnace section is presented in Figure 3.

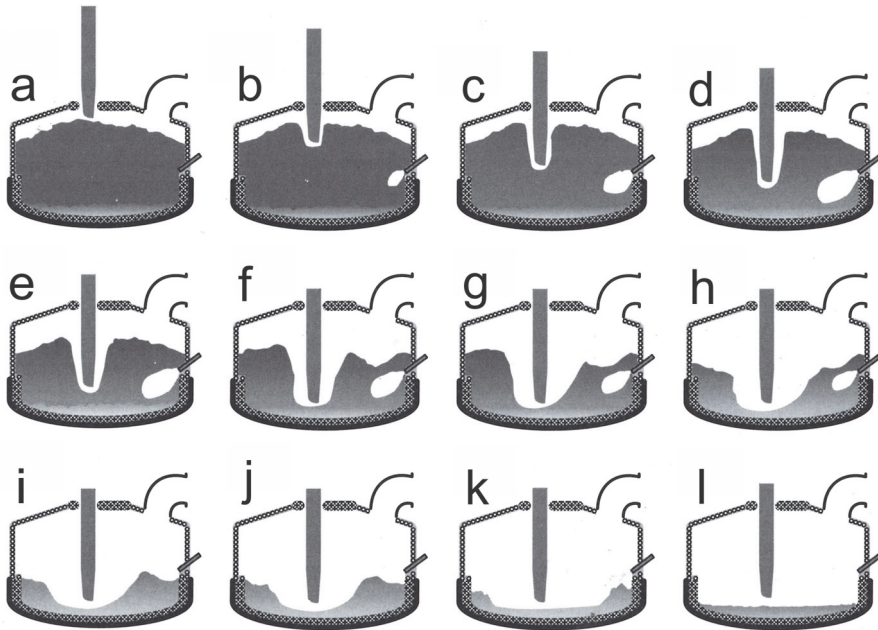


Fig. 3. Melting profiles for a diametrical section through the centre phase (modified from [15], process periods labelled from a to l).

Arc voltage is kept low at the beginning of the melting when the arc is on the top of the scrap (Figure 3 a). The electrodes are lowered continuously when the scrap melts under the electrodes, which causes the arc to be immersed in the scrap (Figure 3 b – e). The movement of the electrodes is controlled to maintain a fixed arc length. When the electrodes are bored inside the scrap, the arc power can be increased because the radiating energy is absorbed by the scrap around the arc. When the electrodes gets near the EAF bottom lining, a liquid pool starts to form on the bottom of the EAF. When the arc reaches the liquid pool, the boredown of the electrodes stop (Figure 3 f). In this phase the maximum arc power can be used because the arc is completely shrouded by scrap and the stability of the arc is ensured by the liquid pool.

After the boredown, the liquid pool forming on the furnace bottom melts the scrap (Figure 3 g). Local scrap melting conditions depend on the number of electrodes; with a three electrode AC furnace the scrap melts first from the three hot-spots between the electrodes and the furnace lining. With multiple electrodes, the arcs curve away from the furnace centre. Between the electrodes and the furnace

lining are the so-called cold-spots, which are not heated as intensely by the arcs as the hot-spots. The movement of arcs in EAF due electromagnetic forces is presented in Figure 4.

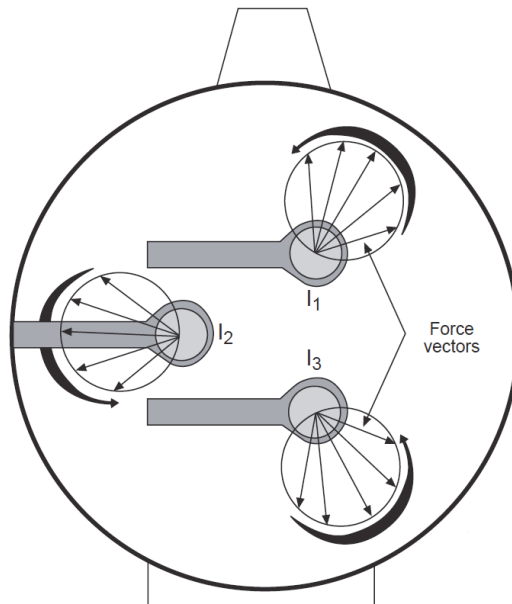


Fig. 4. Electromagnetic forces in an AC electric arc furnace (modified from [14]).

When scrap melts in the hot-spots, the electric arcs become visible from the furnace sides (Figure 3 i). This phenomenon increases the radiation losses, increases refractory wear and decreases the energy efficiency, since a higher amount of energy is transported to water-cooled panels. To decrease thermal load on side panels, the length of the electric arcs is shortened by decreasing the arc power [14]. The heat transfer between arc and furnace sides can also be reduced by immersing the arc in foaming slag. When most of the scrap is already melted, the steel melt is heated to the tapping temperature with low power.

When the scrap charge has melted and reached tapping temperature (Figure 3 l), the melt can be poured out of the furnace to the transfer ladle. Slag can be blown out of the slag door before EAF tapping or tapped in together with steel. The tapping can be conducted through the tapping hole in the furnace side or in the furnace bottom; in stainless steelmaking tapping through side holes is more common than bottom tapping since side tapping increases mixing between slag and steel and promotes reduction of Cr_2O_3 in slag [16].

3.3 EAF auxiliary equipment

EAF auxiliary equipment is usually used to inject solids or gases to EAF [14]. Injection is conducted with a manipulator through the furnace door or with sidewall mounted fixed injectors.

In high productivity EAF process, a part of the inserted energy is supplied as a chemical energy to reduce the electricity consumption and to decrease tap-to-tap times. Chemical energy can be inserted by two methods, by using natural gas burners or oxygen blowing. Burners are typically installed on the furnace sides and the natural gas is injected through a hole in the cooling water panels [1]. Burners are used in the early periods of EAF process to heat the scrap in the cold-spots near the melting point. The input of energy on the cold-spot reduces the melting times of the scrap in places where it last melts, thus reducing the differences between melting of the scrap in the different parts of EAF.

The second method to introduce chemical energy to EAF is to blow oxygen into liquid steel in order to obtain a reaction with dissolved carbon. Oxygen blowing can be conducted using the same equipment as natural gas injection or with a separate oxygen lance through the slag door or tapping hole. Oxygen injection is started after a liquid pool has been formed. Oxygen is injected through the slag into the steel melt, where it reacts with dissolved carbon generating carbon monoxide bubbles. Oxygen blowing also locally oxidizes iron in the steel melt generating FeO, which is reduced by dissolved carbon to further enhance CO generation [17]. Carbon monoxide enters the furnace atmosphere when the bubbles reach the top of the slag and burst.

Blowing oxygen and carbon into carbon steel melt promotes slag foaming. When the generation of carbon monoxide is high enough and properties of the slag are optimal, foam bubbles are formed on a solid layer of slag [17]. The foaming slag has a higher volume than original slag, which causes the slag level to rise and the electric arc submerges in the slag layer. The submerged arc has high energy efficiency, because the radiation from the arc is intercepted by the foaming slag. Therefore, foaming slag enables the use of high arc power even in the later stages of the EAF process, when the scrap has already melted. By stable foaming it is possible to achieve much lower tap-to-tap times while still maintaining high energy efficiency and low refractory wear.

In order to generate foaming slag, the capability of the slag to withhold gas bubbles has to be sufficient, which can be described by the foaming index of the slag. Foaming index can be defined as the change of foam height divided by the

change in the actual gas velocity that is causing the foaming [18]. The most important property affecting the foaming index is the viscosity of the slag; with too low viscosity carbon monoxide bubbles have low residence time in slag. On the other hand, too high viscosity indicates presence of solid particles in the slag, which in excessive amounts break the foam bubbles [19].

3.4 Stainless steelmaking EAF

The main difference between producing carbon and stainless steel grades in EAF is the presence of chromium in stainless steel melt. Chromium has a higher affinity to oxygen than iron, which causes it to react with oxygen when the carbon and silicon levels of the steel melt are locally low enough. This causes the stainless steel slag in the EAF to have chromium oxides in it, which affects the properties of the slag. The solubility of chromium oxides in slag is low, which produces solid precipitates containing CrO_x in slag [20]. The presence of solid particles increases the apparent viscosity of the slag. A small increase in apparent viscosity will increase the foaming index of the slag, but a large amount of CrO_x particles will decrease the foaming index [21].

As the foaming index of the slag depends on the amount of solid CrO_x particles in slag, using the foaming slag practice in stainless steelmaking requires good control of the slag's mineralogical composition [22]. The narrow mineralogical window for optimum foaming index combined with relative slow CO generation in CrO_x reduction [21] makes slag foaming with carbon and oxygen blowing difficult in stainless steelmaking.

3.5 On-line data of EAF

On-line data of the EAF process can be acquired, for example, by measuring thermal conditions of water-cooled panes, arc voltage, off-gas temperature, electrode position, off-gas composition, acoustic emissions or by using sampling probes. The main difficulty in obtaining on-line data of EAF is that the maintenance requirement of sensors can be high, as the EAF environment is very hazardous to measurement equipment. In addition, the current methods cannot reliably measure the most important metallurgical process indicators, i.e. on-line steel temperature or on-line slag composition [1].

Immersion type thermocouples and sampling probes

The traditional method for obtaining information on steel temperature, steel composition and slag composition during the EAF process is the use of immersion type thermocouples and sample probes. Sample or temperature probes are immersed into the melt to obtain discrete information of the said EAF process parameters. The challenge in using sample probes is that the samples are usually not analysed *in situ*, which makes the analysis times usually so long that the results of the composition analysis cannot be used in process control. Recently, robotic systems to conduct temperature measurements have been proposed [23]. One method to obtain a sample of EAF slag is to take the sample from the ladle after EAF tapping. However, the slag composition after tapping does not reflect slag composition in EAF, as reduction of CrO_x occurs in tapping [24].

Thermal conditions in water-cooled side panels

The upper parts of the EAF walls and EAF roof do not have any lining, but are lined with water-cooled panels. Measuring the temperature increase of cooling water enables the analysis of furnace heat transfer. The heat transfer to water-cooled side panels is highest when there is no scrap or foaming slag between the arc and side panels. On the other hand, the response time of the cooling water temperature measurements is often long, since the slag accumulating on panels causes a kinetic barrier in heat transfer between the cooling water and slag surface. For example, in analysing scrap melting and slag foaming for burner optimization, the response time of cooling water temperature has been deemed too high [25]. Furthermore, the thermal conditions of water-cooled panels may be considerably affected by refractory wear and post-combustion of CO [15].

Although the cooling water energy increase has some delay, it provides valuable information for the analysis of scrap melting and slag foaming. It is one of the most reliable methods to analyse scrap melting in the EAF, because the temperature sensors in cooling water stream require only little maintenance.

Off-gas analysis

EAF off-gas composition can be used in analysing EAF process conditions because it reflects the gas generation conditions in EAF, which in turn are related to combustion and oxidation-reduction reactions occurring inside the furnace. The

off-gas composition can be analysed for example with mass spectrometry [26], tunable diode laser measurement [27], infrared absorption or paramagnetism [28]. In the analysis of oxidation-deoxidation reactions, the most important off-gas components for process monitoring are CO and CO₂. O₂ content of the off-gas is especially important in the analysis of combustion reactions and oxygen injection. On the other hand, nitrogen and argon content of the off gas can be used to evaluate the volume rate of off-gas and air leaks. [26]

Acoustic measurements

Acoustic and acceleration sensors measure the noise or vibration of the EAF vessel generated by the electric arc and its turbulent plasma jet. Acceleration sensors for measuring structure-born acoustic emission must be attached to the furnace mantel, while acoustic sensors do not need direct contact with the mantel.

The signal of acoustic and acceleration sensors are related to the noise generation in arc, as well as the acoustic damping conditions inside the furnace. The acoustic emissions are loudest in the start of the boredown period when the arc is on top of the scrap and unstable. When electrodes bore deeper into the scrap and the arc stabilizes due to formation of liquid slag and the electrode heating up, the acoustic emissions decrease. [15]

When scrap melts, the attenuation by the scrap charge decreases and the intensity of sound emissions reaching the furnace shell increases. Therefore, the structure-born sound emissions can be used to measure scrap melting in EAF [29]. In order to gain an accurate signal of scrap melting, the changes induced by changes in arc voltage have to be compensated with appropriate models.

When a flat bath is formed, slag foaming has a substantial effect on sound emissions. In carbon steelmaking, the starting of slag foaming can be immediately observed from reduced furnace noise even from the operator room. Because slag foaming affects sound emissions, a system for controlling slag foaming based on sound emissions have been proposed [30].

Electrical parameters of the furnace power circuit

Another method to measure changes in arc characteristics is to measure the electrical parameters of the EAF power system. Phase-to-phase voltage and current can be measured from either the primary or secondary system with transformers [15]. Active power can be calculated from voltage and current signals. The

electrical parameters of the arc furnace circuit can be used to assess the arc characteristics, since the arc characteristics dominate the changes in electrical circuit parameters. Approximately 95% of the power taken from the utility is released in the arc [14].

The electrical parameters of furnace circuits are mainly affected by three factors: power supply set-point, the conductivity of the arc plasma and the length of the arc. The effect of arc voltage or current set-point is easy to distinguish since a fixed set-point is used over a certain process period. During melting periods the arc length has the most substantial effect on the electrical parameters of the arc. Since arc length is affected by the distance between the electrode and steel bath, the electrical parameters of the arc are closely related to the electrode position control.

Electrode position

The position of the electrode is controlled by the movement of the electrode mast. The electrode position is controlled to minimize the changes in a set point of selected electrical parameter, for example, arc voltage or arc current. With fixed set-point and slag foaming conditions, the electrode regulation system minimizes the changes in arc length. The automatic control of electrodes is especially important in the boredown period, when the occasional collapsing of scrap can cause a short circuit. [31] Electrode positions can be controlled by proportional controllers, while also more sophisticated neural network based control systems have been proposed [32].

Electrode position is one of the few measurements that gives information about scrap melting in the EAF. The length of the boredown period can be approximated from the movement of the electrodes since electrode movement towards the furnace bottom stops after the liquid pool is reached. However, the electrode position is not necessarily stable in the main melting period because the electrode regulation system reacts to short circuiting caused by falling scrap [15]. The connection to falling scrap enables the electrode position signal to be used to assess how close the scrap melting conditions are to the flat bath.

In flat bath conditions, the electrode position is related to the arc length set-point as well as slag foaming. CO bubbles formed in steel melt during slag foaming can raise steel volume and affect the steel surface [15]. Slag foaming also increases the electrical conductivity of the arc, which means that to maintain constant arc voltage during slag foaming, the length of the arc is increased. Due to the

connection between conductivity of the plasma and electrical parameters, a system for measuring slag compositions based on electrical parameters has been proposed for ladle furnaces [33].

4 Optical conditions inside industrial EAFs

The optical conditions of EAF are important in the analysis of the optical emission spectrum since it defines what part of the EAF emits the measured optical radiation. The transporting medium can be called optically thick when optical depth τ , which is an integral of absorption coefficient over unit length, is much higher than 1 [10]. If the transmitting medium is optically thick, it can affect the optical emission spectrum by absorbing the optical radiation emitted farther away from the measurement head or emit radiation of its own.

The radiation from the core of the electric arc must pass through the cooler outer plasma of the electric arc and EAF atmosphere to reach the furnace sides. In these two regions the main mechanism of absorption and emission differs; in the arc plasma the main absorption mechanism is the absorption of atomic emission lines by cooler atoms in the outer plasma, while in the EAF atmosphere the absorption is caused by dust particles.

4.1 Gas composition of EAF atmosphere

Large amounts of gas molecules and dust particles are generated in the EAF process. Particles small enough to be suspended by the gases are called fume [15]. To prevent the off-gas from entering the factory atmosphere, the generated gases are being drawn out of the furnace through a hole in the furnace roof with an off-gas evacuation system [14]. Operating the furnace in low pressure causes the leak air to enter the EAF through openings in the furnace mantel, therefore the EAF atmosphere is a mixture of gases and fumes generated in EAF furnace and the leak air [1].

The temperature and composition of the EAF atmosphere vary in the course of the EAF process. In the early stages of melting, the temperature and composition of EAF atmosphere is mainly affected by the generation of combustible gases originating from the contaminants in the scrap charge and the possible use of natural gas in scrap heating [26]. Scrap charge contains organic compounds, for example oils or greases, which generate volatile organic compounds (VOC) when the temperature of scrap charge increases [14]. The generated VOCs can combust in the presence of leak air, thus increasing the temperature of the EAF atmosphere. Another common contaminant in scrap charge is water, which can directly vaporize to EAF atmosphere or create H_2 gas by reacting with dissolved carbon or various carbon bearing materials charged in the furnace.

In the later stages of EAF processing, the composition of the EAF atmosphere is affected by carbon and oxygen injection. Carbon injection increases the ratio of CO/CO₂ in off-gas, while oxygen injection decreases it. Distinguishing the effect of a single operational parameter in off-gas composition can be challenging because the effects of different operational parameters and process phenomena superimpose each other [26].

The gas molecules inside EAF absorb radiation due to vibration or rotation of their molecular bonds. The absorption of gas molecules is influenced by the temperature and composition of the gas medium. However, the effect of absorption by gas volume on the heat transfer in the CO-rich atmosphere is small [34]. The absorption of gas volume can be neglected when furnace atmosphere contains a significant amount of dust and fume [15, 35].

4.2 EAF Dust

The optical properties of EAF dust is affected by its particle size. Particles with small diameter, especially those of below 1 micron, are effective in scattering and absorbing radiation because of their large surface area to mass ratio. Larger diameter particles are relatively ineffective in scattering and absorption. [15] Therefore, the optical thickness of EAF atmosphere depends both on the amount and particle size of the dust generated in the furnace.

EAF dust can be analysed by taking samples from the EAF off-gas filter system. Chemical composition, mineralogy and particle size of EAF filter dust has been reported in many papers [36 – 40]. Unfortunately, the samples gathered from the filter system do not represent the dust in the EAF atmosphere, as dust particles gathered from off-gas filters can be in liquid form in the EAF atmosphere and the particles have been observed to agglomerate in the off-gas system [15]. The particle size and composition of EAF dust depends on the operational parameters of EAF. The chemical composition of EAF dust varies significantly depending on the reference, as can be observed from Table 2.

Table 2. Chemical composition of EAF dust in various references [41].

Component	Chemical composition by reference								
	[36]	[42]	[38]	[43]	[39]	[44]	[45]	[37]	[46]
Zn	33	29	11.12 – 26.9	24.8	19.4	31.2	13.6	12.2	20.5
Fe	26	25	24.9 – 46.9	32	24.8	18.3	29.8	37.1	21
Pb	3.05	4	1.09 – 3.81	1.84	4.5	1.02	0.69	1.72	4
SiO ₂	3.15	3	–	1.4	3.41	–	–	–	0.4
Cu	0.24	0.3	0.06 – 2.32	0.02	–	–	–	0.17	0.38
Cd	0.05	0.07	0.03 – 0.15	0.03	–	–	0.02	0.01	0.18
Cr	0.24	–	0.06 – 0.58	–	–	0.19	0.09	0.22	0.19
Al	0.6	–	–	–	–	0.68	–	0.41	0.6
Mn	1.83	3	2.46 – 4.6	3.31	–	2.2	–	–	2.25
Ca	2.9	–	1.85 – 10	4.08	–	15.6	–	–	12.5
Na	1.03	–	0.29 – 2.31	–	–	3.8	–	–	1
K	0.85	–	0.06 – 1.12	–	–	0.67	–	–	0.68
Sn	0.024	–	–	–	–	–	–	–	–
Sb	0.06	–	–	–	–	–	–	–	–
Cl	0.011	4	0.51 – 2.36	–	–	–	–	–	3.8
F	0.073	–	0.01 – 0.88	–	–	–	–	–	–

4.2.1 Dust generation

The generation mechanism, particle size and amount of EAF dust differs in scrap melting, liquid bath and foaming slag conditions. The formation mechanisms of EAF dust are [47]:

1. Volatilization by arc or oxygen jet zone
2. Emission of droplets by the arc or oxygen jet
3. Projection of droplets by bursting of CO bubbles
4. Bursting of droplets in EAF atmosphere
5. Direct fly-off

Visual observations indicate that the densest fume is generated in the scrap boredown and melting period [15]. The predominant mechanism of dust generation in the boredown period is proposed to be the interaction between the arc jet and the melting material, which produces liquid iron droplets that later oxidize to iron oxides. The fumes generated in the initial scrap bucket charging originate from the organic material in the scrap charge or fine particles already present in the scrap charge being lifted by charging plume and off-gas evacuation. [15] Incorrect

charging of slag formers and other charge material with small particle size can increase the amount of dust entering off-gas evacuation system [40].

In flat bath or partly covered arc conditions, the predominant cause for dust generation are the gas jets produced by the arcs, burners and oxygen lances, which generate splashes of metal and slag. The smallest particles generated in the splashing exit the furnace via off-gas evacuation system and the larger particles fall back to the melt. [15] The gas jets increase the amount of gas bubbles in the slag and steel, which significantly increases the dust formation because the bursting of gas bubbles on the steel surface is the main dust formation mechanism in EAF [47].

In foaming slag conditions, the splashing caused by the arc, burners and oxygen lances is suppressed by the high volume of slag. Dust particles are being generated due to bursting of bubbles in the foaming slag, but the fume density has been observed to be the lowest in foaming slag conditions. [15]

4.2.2 Optical thickness of EAF atmosphere

With high fuming conditions, the EAF atmosphere is optically thick, which means that photons travel only a small distance in the EAF atmosphere before being affected by the collisions with the particles in the atmosphere. Therefore, in optically thick conditions, the measured optical emission only represents the EAF atmosphere close to the device gathering the optical emissions from the furnace. The high optical thickness of the EAF atmosphere prevents the optical emission from scrap, slag or arc from reaching the analysis equipment.

The optical thickness of the EAF atmosphere has not been extensively studied, although it has a significant effect on heat transfer in the EAF atmosphere. Calculations made by Bowman [15] indicate that the absorption depth, i.e. the distance in which the radiation has been decreased to 37% of its initial value, is in order of 1 m, which means that there is no direct heat transfer between the arc and sidewalls. It can be observed in Table 3 illustrating the effect of fume on power transfer in EAF that the high fuming conditions can reduce the power loss of the bath more than 71%. However, many of the proposed heat transfer models assume that the EAF atmosphere being optically thin [48 – 50], while few include the absorption of furnace atmosphere [15, 35].

Table 3. Effect of fume and post combustion (PC) on heat transfer between different parts of the furnace [15].

State of interior	Bath (MW)	Roof (MW)	Walls (MW)
No fume	-7.3	3.3	4.0
Fume at 16.5 g/m ³	-6.2	3.3	5.0
Fume at 49.5 g/m ³	-2.1	1.2	1.7
Fume at 16.5 g/m ³ + PC	-3.2	0.4	9.0
Fume at 49.5 g/m ³ + PC	0.9	4.2	5.7

Combustion reactions in the EAF atmosphere can affect the measured optical emission through high optical thickness or through generation of heat during combustion. Flames with high optical thickness absorb the optical radiation emitted from the hot steel and slag, while also emitting a high amount of thermal radiation. This causes the optical signal emitted from the furnace to mainly reflect the thermal radiation from the flame.

In order for the flame to be optically thick, solid or liquid surfaces have to be present in the flame. Simple gaseous compounds only absorb radiation of wavelengths specific to the excitation of their molecular bonds, which causes the photons of wavelengths different from these energy levels to pass the material. Optical thickness of flame is increased by the dust particles and the products of incomplete combustion entering the flame, which means that all flames in the EAF are not necessarily optically thick. It is possible for the natural gas flames of the burners to have low optical thickness because of complete combustion due to simultaneous injection of oxygen. On the other hand, the flames related to the combustion of CO have high optical thickness, since the formation mechanism of CO includes the bursting of CO bubbles on the steel surface, which is an important dust formation mechanism.

When the temperature of a flame is high enough, it can affect the measured optical emission spectrum even if the optical thickness of the flame is not high. With a high enough temperature, even the few particles in the relatively optically thin flame will emit a high amount of thermal radiation, which will affect the measured optical emission spectrum.

As discussed earlier, the requirement for the high optical thickness in the EAF atmosphere is the presence of dust particles. This means that the changes in dust generation during the EAF process affect the optical thickness of the EAF atmosphere during different process periods. The dense fumes formed in the boredown period and early main melting period can be completely opaque to

wavelengths of visible light, thus blocking the optical emissions from the EAF completely. The exact phenomena causing the formation of dense fume is not known; it has been suggested that it originates from interaction between the arc jet and solid scrap, as well as formation of soot in incomplete combustion of VOCs [15].

4.2.3 Significance of optical thickness in optical measurements

The optical thickness of the EAF atmosphere limits the optical measurements of the arc, slag and scrap in the early process periods when the fume formation is high. Previously, the problem of flames with high optical thickness has been solved by measuring infrared wavelengths, which have higher optical depth than visible wavelengths in flames with high amount of dust [51]. On the other hand, it is very difficult to measure the optical depth, as the fuming conditions change from EAF to EAF and from process period to another. In basic oxygen converters, the particle emissivity of the off-gas has been found to fluctuate between approximately 0.2 and nearly 1 depending on the temperature and the amount of carbon in steel [6]. Earlier studies by Bowman [15] have suggested that the optical depth of the EAF atmosphere is much lower than the diameter of the EAF, thus in effect blocking a major amount of radiation emitted by the arc. However, this was not found to be the case in industrial DC arc furnace measurements conducted by Block [9], in which optically thin Fe I lines were used in plasma temperature calculations. In conclusion, the optical thickness of EAF atmosphere can vary significantly, and optical thickness of the EAF atmosphere must be taken in account if the optical emission spectrum measured from slag or scrap is analysed.

4.3 EAF arc plasma

Arc plasma generated between the carbon electrode and steel bath can be described as a cylinder shape, in which the temperature is highest in the middle and is lower in the outer edges of plasma. An AC arc fluctuates according to the sinusoidal changes in power supply, which usually occur at a frequency of 50 Hz. During each cycle, the arc will initiate and fade. On the other hand, the static expression of electric arc plasma is not accurate even for static power supply DC arc plasma, as demonstrated by Jones et al [52]. Arc plasmas of different shapes can be observed in Figure 5.

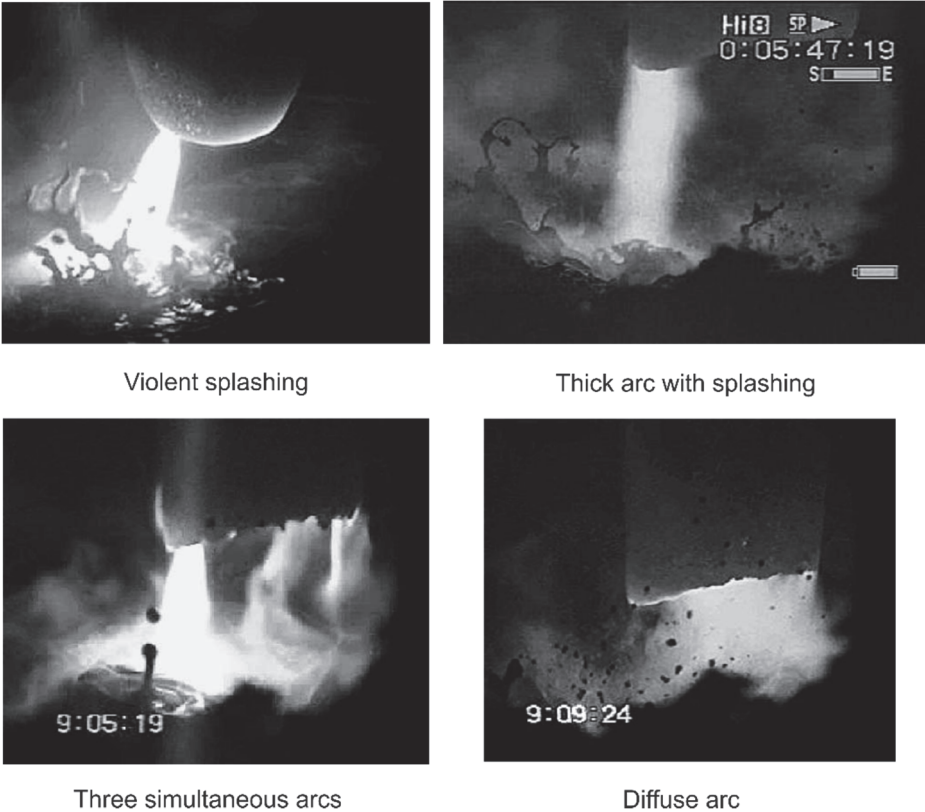


Fig. 5. Examples of different arc shapes observed in DC arc furnace (modified from [52]).

4.3.1 Validity of LTE assumption in industrial furnaces

Validity of the LTE assumption is important in selecting an appropriate model for the arc plasma. In LTE plasma collisions with electrons must dominate radiative processes, which require sufficiently high electron density [11]. The assumption holds in the core of the arc plasma, but it does not hold at the outer edges of arc plasma, near cathode and anode regions or anywhere in AC arc when the arc current passes zero [53, 54]. In plasma modelling, the non-LTE conditions in cathode and anode regions can be modelled by using sub-models suitable for non-LTE conditions [55]. On the other hand, it is not reasonable to use non LTE methods with simple measurement of line intensities when plasma characteristics are calculated from the optical emission spectrum [56].

4.3.2 Plasma temperature

Electron temperature is the most important parameters of the arc plasma when the optical properties of arc plasma are studied. It significantly affects the absolute and relative line intensities of atomic and ionic emission lines. Electron density affects the shape of the atomic and ionic emission lines through line broadening. The temperature distribution of the EAF arc plasma has been calculated in numerous studies for AC and DC arcs using various models [54, 55, 57 – 61]. An example of calculated temperature distribution of the arc plasma is presented in Figure 6.

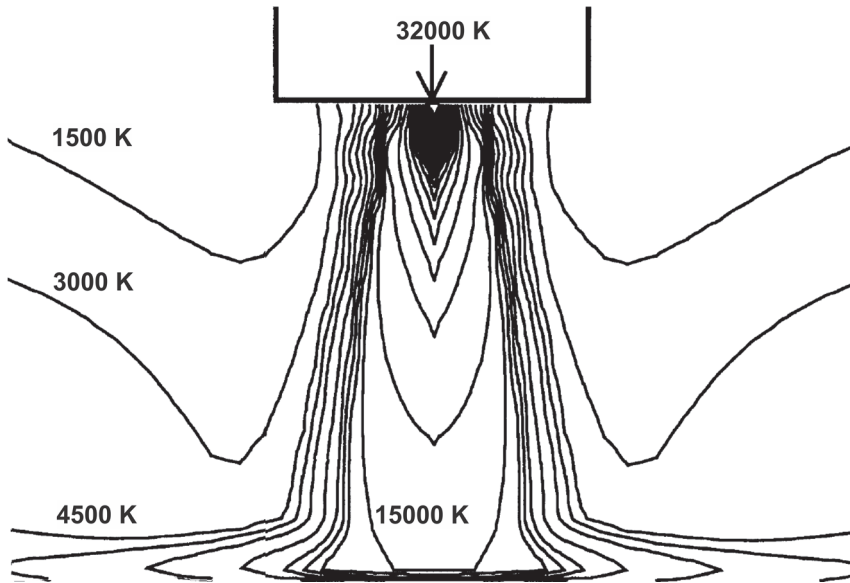


Fig. 6. Example of modelled temperature distribution in dc arc plasma (modified from [59]).

4.3.3 Optical thickness of arc plasma

Optical thickness of the arc plasma affects the heat transfer from plasma to furnace sides. Optical emissions from the plasma core can be absorbed or scattered in the cooler outer edge of the plasma. Absorption and scattering are caused by many different phenomena related to the interaction of emitted photons with the matter and other photons in the outer edge of plasma. High optical thickness of plasma changes the amount and wavelength of photons emitted from the core of plasma and causes the optical emission spectrum of arc to describe the optical emission spectrum of the outer arc plasma (Figure 7). High optical thickness of arc plasma is beneficial to EAF process because it prevents direct heat transfer between the core of the plasma and furnace sides.

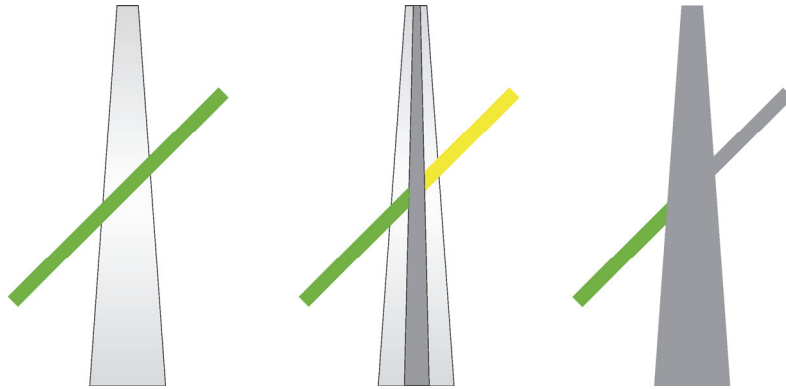


Fig. 7. Optically thin (left), partially optically thick (middle) and optically thick (right) plasma (modified from [15]).

The high electron temperature of the plasma causes more photons to be emitted and increases the probability of photons undergoing collisions in the outer plasma. Therefore, the optical thickness of the plasma will increase as the plasma temperature increases. However, absorption probabilities are different for all atomic emission lines because the amount of emitting species in plasma and the transition probability of atomic emission lines affect the absorption probabilities. Because the amount of atoms of emitting species is difficult to measure, the main focus in measuring the optical thickness of arc plasma has been in defining the plasma temperature limit of optically thin conditions in arc plasma. Even these kinds of measurements and models studying the optical thickness of the plasma are scarce and contradictory. The cross-over between optically thick and thin conditions for Fe I lines have been calculated to happen between 3000 K and 7000 K by Bowman [62]. On the other hand, the plasma temperature in an industrial DC furnace has been calculated as between 7400 K and 9700 K from Fe I lines with low uncertainty, which suggests that Fe I lines can be at least somewhat optically thin in these temperatures [9]. The possible explanation for these seemingly contradictory results would be the optical thickness depending highly on the position of the arc, which has been observed by Veilette & Simard [8] in ilmenite smelting DC furnaces.

4.3.4 Modelling heat transfer from arc plasma

The heat transfer from electric arc plasma can be simplified in heat transfer models by assuming it emits thermal radiation as a grey body and is optically thin [58, 63].

While the grey body assumption greatly simplifies the heat transfer, it is not completely accurate since the emissivity of varies significantly between different wavelengths, because a major part of the radiation is emitted through the atomic emissions. Recently, in some EAF plasma models the radiation from the atomic emission lines of iron has been included by using a net emission coefficient [62, 64]. The Fe I net emissions coefficient describes the sum of radiative power from Fe I lines over the whole wavelength range. Line radiation from other atoms have been included in radiation models for ferrosilicon production furnaces [65, 66]. To the knowledge of the author, no EAF arc plasma models have included the effect of other metallic vapours besides iron.

5 Experiments

The use of optical emission spectrometry in on-line in situ process control was studied by conducting tests in laboratory, pilot and industrial furnaces. The laboratory furnace used in the measurements reported in Paper I was situated in the laboratory of the Electron Spectroscopy Group, University of Oulu. The pilot AC furnace used in measurements reported in paper II was situated at the Department of Industrial Furnaces and Heat Engineering, RWTH Aachen University. The industrial measurements reported in papers III and IV were conducted at Outokumpu Stainless Oy, Tornio Works, EAF 2.

5.1 Laboratory furnace

In Paper I, the EAF slag emission spectrum was measured from a laboratory version of a DC arc furnace. The furnace configuration is shown in Figure 8. The arc was produced between two graphite electrodes fixed to water-cooled copper conductors. The sample was placed in a graphite crucible and inserted into the furnace from below. Light passed through a fused silica furnace window and was collected with an optic fibre.

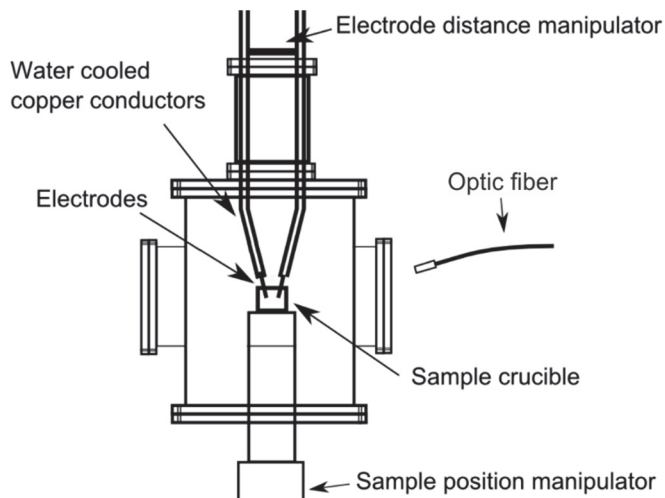


Fig. 8. Schematic figure of laboratory furnace [Paper I, reprinted by permission of Applied Spectroscopy].

A Kemp Stick Master 1400 welding machine was used as the power source for the arc. The welding machine enabled control of the arc current, but the arc voltage varied depending on the distance between the electrodes. Voltage fluctuations were induced by selecting a fixed arc current and changing the electrode distance manually. The voltage fluctuations were simulated in the fixed arc currents of 50, 75 and 100 A.

The furnace chamber was purged with argon gas. The measurements were conducted by first initiating the arc with a short electrode distance and then increasing it. After increasing the electrode distance the sample crucible was raised to the arc. The device is described in detail by Mäkinen [67].

5.1.1 Measurement equipment

A commercial Czerny-Turner spectrometer Andor Shamrock i500 with the grating enabling measurement of the widest possible spectral range (245 – 610 nm) was used in the measurements. The selected grating had 150 lines/mm (300 nm blaze) and it was used with a 10 μ m slit. This grating along with CCD provided a pixel to pixel resolution of 0.1782 nm and an optical resolution of 0.525 nm. The widest possible spectral range was chosen since gaining information about as many atomic emission lines as possible was deemed more important than the accuracy of a single atomic emission line. The spectrometer was used in high-capacity readout mode which provided a readout rate of 50 kHz at 16-bit. Integration time was set to 0.0021 s.

5.1.2 EAF slag samples

The measurements reported in Paper I were conducted on samples of industrial slag. The EAF slag samples were obtained from the two EAFs at Outokumpu Stainless Oy, Tornio Works. The samples were taken from the ladle after the EAF tapping and crushed to maximum grain size of 10 mm.

The particle size and mineralogy of the samples was found to vary significantly. Some samples had shards of nearly one centimetre in length while some were the size of very fine sand, as can be observed in Figure 9.

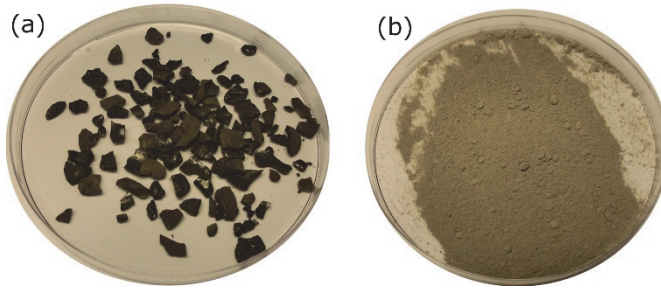


Fig. 9. Macroscopic observations of slag samples (a) shards (b) sand [Paper I, reprinted by permission of Applied Spectroscopy].

Five of the samples were obtained from production line 1 and the rest from line 2. Table 4 shows the X-ray fluorescence (XRF) analysis of slag composition. All oxides of iron and chromium with different oxidization states are summed to the amount of Fe_2O_3 and Cr_2O_3 . Minor slag components have been removed from the results of the analysis.

Table 4. XRF analysis of slag samples [Paper I, reprinted by permission of Applied Spectroscopy].

Production line	Sample number	Cr_2O_3	Fe_2O_3	Al_2O_3	MgO	CaO	SiO_2	MnO	TiO_2
1	1	7.8	1.5	3.8	6.3	44.4	28.1	3.0	1.7
1	2	8.6	1.5	4.6	4.1	39.7	32.5	4.4	2.2
1	3	5.2	1.7	9.4	9.8	30.4	31.4	2.7	2.9
1	4	7.6	1.6	7.8	8.6	31.8	31.1	4.4	2.1
1	5	5.4	1.3	4.4	6.3	42.5	30.5	2.9	2.1
2	6	2.1	1.3	10.0	4.4	53.5	23.4	0.7	2.9
2	7	2.0	1.4	10.1	4.3	53.4	23.6	0.6	2.4
2	8	2.3	1.2	14.4	5.3	43.3	25.3	1.5	2.7
2	9	8.6	1.3	14.3	3.9	39.6	23.5	3.3	2.2
2	10	8.5	1.4	15.8	3.7	39.8	22.7	3.1	2.2
2	11	8.0	1.4	15.4	3.9	39.6	23.5	3.0	2.3
2	12	5.6	1.5	10.5	4.6	44.7	24.4	2.6	2.0
2	13	7.9	1.6	9.1	4.8	46.1	23.3	2.3	1.9
2	14	2.5	1.2	9.5	5.5	47.9	25.9	1.4	1.9
2	15	2.5	1.3	16.8	6.1	40.7	24.5	1.4	2.2
2	16	5.0	1.5	9.5	8.0	40.3	26.1	1.8	1.8
2	17	4.7	1.3	8.4	7.7	41.3	27.0	2.3	2.0
2	18	2.2	1.3	11.8	9.1	37.4	27.2	1.5	3.1

5.1.3 Correction of spectral data

The spectrum obtained from the spectrometer contains distortions caused by the quantum efficiency of the CCD, the efficiency of the grating and the transmission of the optic cable. These were corrected according to data provided by the manufacturers of the equipment. Also, due to the dark current in CCD, a certain background intensity can be observed even if there is no light coming to the spectrometer. The removal of the dark current was performed by measuring the spectrum with the aperture closed and removing the reference spectrum from all the measured spectra of the electric arc. The thermal radiation was removed by approximating it with a fit curve and subtracting the curve from the spectrum. The photon flux caused by thermal radiation was approximated with the equation:

$$M(\lambda, T) = \frac{2\pi c}{\lambda^4 \left[e^{ch/\lambda kT} - 1 \right]} \quad (3)$$

where M is the photon flux, T is the temperature in degrees Kelvin, h is the Planck constant, c is the speed of light, λ is the wavelength in nm and k is the Boltzmann constant [68]. It is difficult to estimate the average temperature near the electric arc, so the photon flux curves were calculated for different temperatures according to Eq. 1 and the best fitting curve was selected. The photon flux curves were calculated with temperature interval of 5 K. The selection of the best fit curve was performed by proportioning the curve to the local minimum near 509 nm and selecting the fit curve with the lowest sum of square differences of minimums in the wavelength ranges 465 – 482 nm, 425 – 445 nm and 515 – 526 nm. Figure 10 presents an example of a raw spectrum for 75 A measurements and its photon flux fit. The average of the last 15 corrected frames was deemed to represent each sample in the correlation analysis.

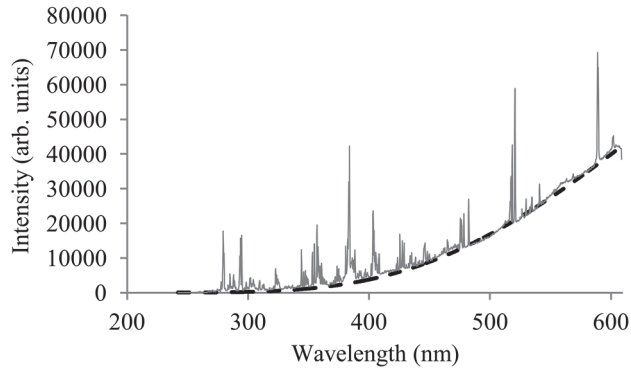


Fig. 10. An example of fitting photon flux curve to emission spectrum [Paper I, reprinted by permission of Applied Spectroscopy].

5.2 Pilot-scale EAF

5.2.1 Furnace description

The experiments reported in Paper II were performed at an airtight pilot arc furnace which simulates the operation conditions of industrial scaled arc furnaces. The pilot furnace was situated at Aachen RWTH University in Germany. The furnace is water-cooled and it consists of a fixed top reactor and a moveable crucible with a maximum capacity of about 200 kg of steel melt. It is possible to operate the furnace in AC-mode with two electrodes or in DC-mode with one top electrode and an anode in the bottom of the crucible. In AC-mode the maximum active power is 600 kW and in DC-mode 300 kW. The experiments in Paper II were carried out using the AC-mode. The furnace transformer has a rated power of 850 kVA, the secondary voltage is adjustable in 10 steps from 250 to 850 V and the maximum arc current is 2 kA.

5.2.2 Measurement system description

The measurement system consisted of a measurement head, an optical fibre approximately 10 metres in length, a spectrometer and an analysis computer. The measurement head was an approximately twenty centimetre long stainless steel pipe with an aperture for the optical fibre. The measurement head was installed in the injection tube in the furnace shell, which had direct vision to the other electric

arcs. The position of the arc was verified through visual observations. The measurement configuration yielded a measurement cone of 15 cm in the approximate position of the electric arc.

A Thorlabs 600 μm fibre 10 metres in length was used in the measuring system. The spectrometer used was Avantes Avaspec ULS3648 with a 10 μm slit, 500 nm blaze and spectral range of 400 nm to 900 nm. The spectrometer configuration had an optical resolution of 0.3 – 0.36 nm, and the integration time was 5 ms or 10 ms depending on how much light was emitted from the arc. CCD based averaging to 500 ms was used to reduce dark noise.

5.2.3 Test period description

Two heats with varying CrO_x content of the slag were measured. The furnace was first loaded with stainless steel and carbon steel scrap, anthracite and slag formers. After the first batch was partially melted, more stainless steel scrap and more slag formers were charged in furnace. After the second batch of scrap had completely melted, the actual measurements were started. During the measurements the optical emission spectrum of the electric arc was continuously measured while the CrO_x content of the slag was increased by subsequent additions of Cr_2O_3 powder. The additions were conducted by opening the furnace and mixing Cr_2O_3 powder to the slag. Before each addition of Cr_2O_3 , a slag sample was taken with a sampling cup and cast to a sample holder. In between Cr_2O_3 additions the melt was heated for approximately seven minutes to supply the energy lost in opening the furnace and to let the Cr_2O_3 powder to mix and dissolve to slag.

The same amount of slag formers were added to both test heats. The aim of the starting slag composition was MgO 10.0 wt-%, Al_2O_3 19.0 wt-%, SiO_2 29.0 wt-%, CaO 42.0 wt-%. The XRF analysed slag compositions are presented in Table 5. The slag composition was defined so that low viscosity slag with low melting point was obtained along with sufficiently high basicity. The slag formed in the beginning of heat was defined to have liquidus temperature below 1500 °C. It can be observed in Table 5 that the Cr_2O_3 content of the slag increases during the heats, which was the purpose of the Cr_2O_3 additions. It is interesting to note that the amount of FeO in slag differs in both heats. This is likely caused by differences in steel composition and varying amounts of anthracite additions.

Table 5. Aim of the starting slag composition and the results of XRF analysis (wt-%) [modified from Paper II].

Heat – Sample	MgO	Al ₂ O ₃	SiO ₂	CaO	Cr ₂ O ₃	MnO	FeO
Heat 1 – Sample 1	8.50	15.00	30.88	35.70	3.44	2.65	1.79
Heat 1 – Sample 2	8.54	15.03	30.76	35.29	4.37	2.73	1.75
Heat 1 – Sample 3	8.61	14.93	30.67	35.10	5.10	2.76	1.56
Heat 1 – Sample 4	8.44	14.69	30.62	34.39	6.62	2.78	1.66
Heat 1 – Sample 5	8.37	14.46	29.94	33.49	8.59	2.79	1.95
Heat 2 – Sample 1	8.97	15.10	29.18	33.88	7.03	2.31	2.51
Heat 2 – Sample 2	9.10	14.62	29.22	33.43	7.69	2.37	2.71
Heat 2 – Sample 3	8.91	14.42	29.02	33.32	8.29	2.36	2.77
Heat 2 – Sample 4	9.02	14.21	28.65	32.75	9.23	2.33	2.92
Heat 2 – Sample 5	8.71	13.96	28.89	33.08	9.25	2.29	2.95
Heat 2 – Sample 6	9.11	13.75	27.92	31.91	11.3	2.27	3.03

5.2.4 Data handling

Data was acquired by an in-house spectrum analysis software EAFSA. This analysis software makes use of a prebuilt ROOT library [69]. Spectral distortions were removed according to the data provided by the manufacturers of the optical components. The atomic emission lines were approximated by Gaussian functions. Background curve was subtracted by approximating it with liner fit calculated to the spectrum range near the measured lines.

5.3 Industrial EAF

The measurements conducted in Papers III and IV were conducted at EAF 2 in Outokumpu Stainless Oy, Tornio works. EAF 2 is a 140t AC EAF with bottom gas purging, several burners and an injection lance operated through the tapping hole. During the measurements bottom purging, the burners and injection lance were not used. This minimized the dust and CO generation in the furnace atmosphere and kept the furnace atmosphere as optically thin as possible. The studied production line mainly produces austenitic stainless steels. The compositions of the steel and slag samples obtained from the studied heats are presented in Table 6 and Table 7.

Table 6. XRF analysis of slag samples obtained from the measured heats [Paper III, reprinted by permission of Metallurgical and Materials Transactions B].

Heat	Cr ₂ O ₃	Fe ₂ O ₃	Al ₂ O ₃	MgO	CaO	SiO ₂	MnO	TiO ₂
1	6.6	1.3	6.2	6.1	43.1	26.9	3.6	1.8
2	6.2	1.4	4.9	5.0	43.2	29.9	3.5	1.9
3	12.4	1.6	7.5	4.3	40.8	23.5	4.1	2.4
4	9.3	1.4	8.0	4.0	41.9	25.0	4.1	2.7
5	8.4	1.4	5.8	4.8	42.4	25.9	4.1	2.3
6	13.2	2.0	4.5	5.0	37.2	29.7	4.7	1.4
7	13	1.9	5.3	6.2	38.0	26.7	3.9	1.6
8	9.7	2.6	4.8	7.5	36.7	27.4	3.2	1.6
9	14	1.8	5.9	6.0	32.7	29.1	4.8	2.0
10	11.9	1.9	5.8	5.8	35.1	28.8	4.7	2.0
11	11.3	1.8	5.4	5.7	36.7	29.1	4.5	1.8
12	11.9	1.8	5.1	5.8	36.9	28.8	4.2	1.7
13	9.0	1.6	5.2	6.1	38.7	29.2	4.3	1.8
14	6.7	1.0	6.6	5.7	38.5	30.7	3.7	2.0
15	6.9	1.6	7.5	6.0	38.5	28.4	3.1	2.4
16	5.9	1.4	12.5	5.8	40.6	24.4	3.2	1.6

Table 7. OES/XRF analysis of steel samples obtained from the measured heats [Paper III, reprinted by permission of Metallurgical and Materials Transactions B].

Heat	C	Si	Mn	P	S	Cr	Ni	Mo
1	1.283	0.02	1.08	0.04	0.0212	17.73	9.01	1.77
2	0.865	0.03	0.85	0.031	0.0229	17.85	8.27	2.26
3	1.029	0.18	0.89	0.031	0.0298	17.36	9.28	1.43
4	1.099	0.05	0.92	0.031	0.0257	18.06	9.28	1.52
5	1.160	0.09	0.95	0.037	0.0214	17.72	8.28	1.64
6	0.908	0.33	0.87	0.035	0.024	16.66	8.90	1.82
7	0.489	0.11	0.81	0.033	0.0278	16.29	9.92	1.95
8	1.053	0.18	0.96	0.034	0.0251	16.58	8.87	1.72
9	1.123	0.15	0.68	0.038	0.0472	16.41	9.58	1.99
10	1.164	0.18	0.87	0.034	0.0387	17.88	9.90	2.00
11	1.244	0.07	0.71	0.034	0.0395	17.50	9.02	1.94
12	1.451	0.43	0.82	0.034	0.0377	18.01	8.69	1.79
13	1.191	0.05	0.91	0.034	0.0318	18.39	9.33	1.93
14	1.233	0.23	0.94	0.036	0.0341	18.68	9.32	1.97
15	1.394	0.29	1.01	0.034	0.0342	18.75	9.36	1.94
16	0.993	0.22	1.22	0.03	0.0137	18.90	7.85	0.46

The measurements reported in paper III were conducted in February 2012. The measurement period lasted four days, in which 16 different heats were measured. The measurements reported in paper IV were about one and half year later in July 2013. In the latter, measurements from 70 heats were analysed over a period of one month.

5.3.1 Measurement system

The measurement system for obtaining optical emission spectra from an industrial EAF was roughly similar in both measurements reported in papers III and IV. The schematic picture of the measurement systems for these two measurement periods are presented in Figure 11. The configuration of the measurements systems used in the two measurements are presented in Table 8.

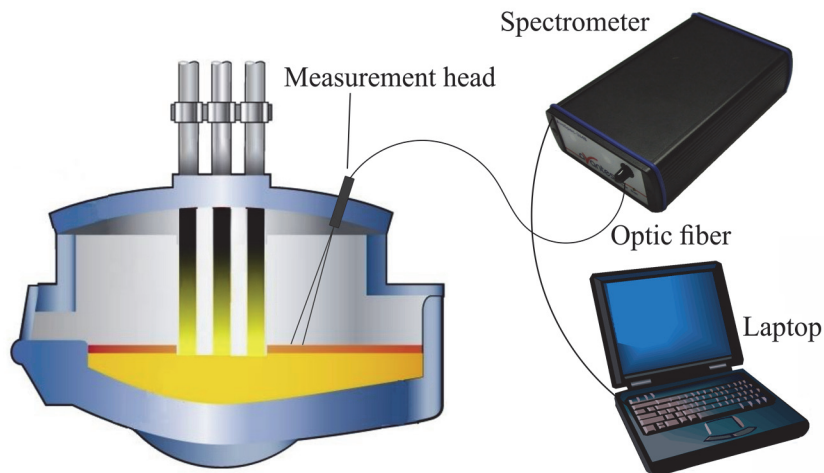


Fig. 11. Schematic presentation of measurement system [Paper IV, [70], reprinted by permission of ISIJ International].

Table 8. Summary of equipment and software used in paper III and IV.

Paper number	Measurement head	Optical fibre	Spectrometer	Software
Paper III	3 mm aperture	Ocean Optics 600 μm	Andor shamrock 500i	Andor Solis and In-house software
Paper IV	5 mm aperture	Ocean Optics 600 μm	AvaSpec-ULS3648	In-house software

The measurement head was installed on the EAF roof in the unused lime injection collar, on the outer edge of the furnace. The same measurement head placement was used in both measurements reported in Papers III and IV. The protection tube was inserted about 10 cm below the top of the lime injection collar.

The measurement head was a steel pipe holding the end of the optical fibre in the middle of it (Figure 12). The hole in the end of the measurement head acted as an aperture for the measurement cone.

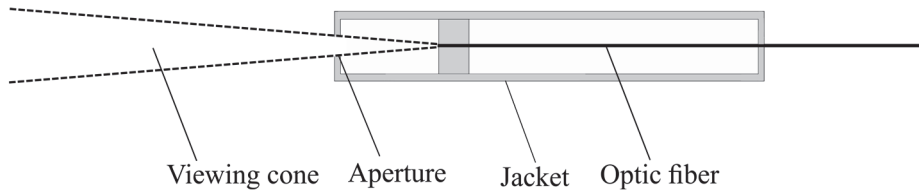


Fig. 12. Schematic picture of measurement head [Paper III, reprinted by permission of Metallurgical and Materials Transactions B].

Air was also blown through the aperture to prevent dust from gathering, to cool the measurement head and to keep slag splashes from reaching the optical fibre. In the measurements reported in paper III the measurement head also had a separate cooling of jacket.

The measured area was defined by the diameter of the aperture in the measurement head and the distance between the hole and the optical fibre. The distance between the optical fibre and the slag surface was approximately four metres. In the Paper III the aperture had a diameter of 3 mm, which yielded a measuring area of approximately 10 centimetres on the slag surface. The hole used in the measurements reported in Paper IV was of 5 mm diameter and the distance to the optical fibre was 15 cm. This configuration provided an optical fibre viewing spot of 15 cm diameter on the slag surface. The aperture was kept small to ensure high air flow without blowing an excessive amount of leak air into the EAF.

The measurement system was found to function well throughout both measuring periods. The protection pipe provided sufficient protection from EAF atmosphere for the optic fibre. Air purging kept the aperture free of slag and the protection tube cold enough to keep the optic fibre intact. No visible wear of the measurement head was observed during the measurement period and slag did not accumulate on it. The good durability of the measurement head was attributed to the lime injection collar being situated near the furnace sides, which are protected by scrap during the boredown period when the splashing of steel and slag are intense. Also, it is worth to noting that the spectrometer and the laptop computer endured strong magnetic fields in the maintenance room under the EAF transformer.

In the longer measurement period reported Paper IV, the only operational problem was the accumulation of slag on the lime injection collar. The accumulated slag created an arch on the lime injection collar and blocked the view to the furnace. The slag blocking the view could only be removed during weekly maintenance.

An Ocean Optics 600 μm optic fibre for ultraviolet (UV) and visible (VIS) wavelengths was used in both the measurements. The spectrometers used in the

measurements was situated at the end of a 30-meter-long optic fibre, which enabled the placement of spectrometer well away from the EAF.

In paper III, the measurements were conducted with an Andor shamrock 500i spectrometer along with a Newton DU940N CCD-camera, which was the same configuration as in Paper I. The CCD was cooled to $-50\text{ }^{\circ}\text{C}$ to ensure low dark current. A grating with 150 lines/mm and 300 nm blaze was used in together with a $10\text{ }\mu\text{m}$ slit. A grating with as broad a spectral range as possible was used to gain information on the overall characteristics of the emission spectra. The spectrometer setup offered an optical resolution of 0.525 nm, which is reasonable considering the wide wavelength range measured (318 – 680 nm). The integration time of each spectrum was 0.5 s, and the kinetic cycle of the measurement was 0.552 s. The integration time being 0.5 s means that a single measured spectrum frame is an average of many supply voltage cycles (about 28 with 50 Hz power supply).

In the measurements reported in Paper IV, an AvaSpec-ULS3648 high-resolution spectrometer was used with 600 l/mm grating (500 nm blaze) and entry slit width of $10\text{ }\mu\text{m}$. The wavelength range of the spectrometer configuration was 300 – 800 nm. The AvaSpec-ULS3648 was chosen instead of the Andor i500 because spectral imaging and changeable grating were not required. In this application, AvaSpec spectrometer provided superior optical resolution (0.3 nm) combined with a simpler spectrometer configuration. The measurements were conducted with a 150 millisecond integration time and an average of 8 frames, which results in a kinetic cycle of 1.2 seconds. Averaging was used to reduce dark noise, which was considerable due to the lack of CCD cooling.

5.3.2 Emission spectrum analysis

The data obtained from the measurements reported in papers III and IV were processed with the same in-house spectral analysis software as in Paper II. The data was analysed by calculating spectrum indicators which approximate the most important spectrum features, namely the average temperature of the viewing cone and the of alkali emission lines. Different indicators and their descriptions are presented in Table 9.

The measured raw spectra contain systematic distortions caused by the transmission of the optical cable, the quantum efficiency of the CCD and the efficiency of the grating. These effects were corrected by normalizing the spectra according to data provided by the manufacturers of the optic cable and the spectrometer.

Table 9. Indicators calculated from the spectrum and their descriptions.

Indicator name	Description	Related process phenomena
Two-point temperature	Temperature of emitting material calculated from relative intensities of two wavelengths	Average temperature of the material in the measuring area
Spectrum average intensity	Average intensity of the whole spectral range	Relative amount of the hot material in the viewing cone and it's emitting
Alkali line intensity	Area of Voigtian of Gaussian function fitted to an alkali peak	Excitation conditions in the measuring area
Alkali line FWHM	Width of the peak calculated at half of the maximum peak intensity	Magnitude of the line broadening
Alkali line absorption coefficient	Area of the negative Voigtian peak fitted to a 589 nm area	Absorption by sodium containing fumes in the EAF atmosphere

The spectrum indicator describing the average temperature of the viewing cone was based on the assumption of the material in the viewing cone being a grey body. The temperature of the emitting material was calculated according to Eq. 4, which can be derived from the ratio of the intensities of different wavelengths according to Wien's law.

$$T = \left(\frac{1}{\lambda_2} - \frac{1}{\lambda_1} \right) \frac{hc/k}{\ln[R(\lambda_1/\lambda_2)^5]} \quad (4)$$

where λ_2 is the wavelength of the second measured intensity band, λ_1 is the wavelength of the first measured intensity band, h is the Planck constant and R is the intensity ratio. The average temperature was calculated according to relative differences in average intensities of 600 nm and 800 nm. The average temperature of the emitting material calculated from the intensities of two wavelengths provides a fast tool for analysing relative differences in spectrum temperature. However, the absolute accuracy of the calculated temperatures relies on the accuracy of the grey body assumption and correction factors of fibre transmission, grating transmission and CCD quantum efficiency. While the optical characteristics of the measurement system are documented by the equipment manufacturers, the accuracy of the grey body assumption is difficult to measure because it requires prior information about the optical characteristics of the slag surface and EAF atmosphere. Because of these uncertainties in the validity of the grey body assumption, the emphasis of the

temperature analysis is on the relative changes of temperature and not the absolute values of the calculated temperatures.

Average spectrum intensity is calculated from intensities of all wavelength bands over the full spectrum range. The average spectrum intensity describes how much light is emitted from the measured area, which is relative to the amount of high temperature matter in the viewing cone. With spectrum intensity and two-point temperature it is possible to draw conclusions about the spatial differences in the temperature of the measured area. For example, high spectrum temperature combined with low average intensity indicates that the high temperature matter encompasses only a small part of the measurement area.

The third indicator in Table 9 approximates the intensity of the atomic alkali excitation lines. The high temperature inside EAFs causes excitation of alkali metals, especially in flames. The alkali lines were approximated with Voigtian or Gaussian functions and the intensity of the excitation lines was measured by calculating areas of the fit curves. The width of the alkali emission lines was approximated by calculating the full width at half maximum (FWHM).

The shape of alkali emission line can be affected by absorption in the furnace atmosphere, which has to be approximated to enable comparison of alkali peaks shapes. The degree of absorption is approximated by fitting a negative Gaussian curve in the middle of the 589 nm region. This method creates some errors in the calculation of absolute line intensities, it but provides a fast tool for analysing relative line shapes.

6 Results and discussion

This study focusses on three different aspects of stainless steelmaking in EAF, which are the analysis of slag composition, characteristics of arc plasma and EAF process conditions. The relation of original papers of this dissertation and their relation to the studied topics are presented in Table 10. The main findings of this work are:

1. Chromium content of the slag can be analysed from the optical emission spectrum of the electric arc in laboratory and pilot scale.
2. Measurement of the optical emission spectrum on an industrial scale is feasible.
3. The optical emission spectrum of the electric arc mainly originates from the vaporized slag components.
4. Ca I emission lines from arc plasma can be optically thin to temperatures of 7 000 K.
5. Optical emission spectrum can be used to evaluate the gas-phase and slag surface conditions in industrial EAFs.

On-line measurement of EAF slag composition from the optical emission spectrum was studied because it would allow dynamic control of slag CrO_x content in stainless steelmaking EAF. Slag composition analysis is supported by obtaining a better understanding of EAF plasma characteristics, which affect the optical emission spectrum obtained. Better understanding of the optical properties of the electric arc also enable accurate modelling of electric arc heat transfer since the optical thickness of the plasma significantly affects the accuracy of heat radiation models. The third topic of the analysis is EAF process conditions. By obtaining information of scrap melting and slag foaming, it is possible to compensate the changes in scrap composition by for example adjusting the arc voltages.

Table 10. Topics of the original papers.

Scale	Characteristics of EAF arc plasma	EAF slag composition	EAF process conditions
Laboratory	Paper I – Analysis of atomic emission lines	Paper I – Analysis of feasibility of slag composition ratios	<i>Not applicable</i>
Pilot	Paper II – Analysis of atomic emission lines	Paper II – Accuracy of analysing slag Cr ₂ O ₃ content	Paper II – Connection between slag composition ratios and chromium in slag
Industrial	Paper III – Calculation of plasma temperature, approximating plasma thickness and composition	Paper III – Feasibility of using optical emission spectra of arc to measure slag composition	Paper III – Evolution of optical emission spectrum during EAF process Paper IV – Optical emission spectrum in analysis of EAF atmosphere, slag surface and scrap melting conditions

6.1 Characteristics of EAF arc plasma

Obtaining more accurate description of the characteristics of arc plasma enables more accurate modelling of heat transfer in plasma. The optical emission spectrum measurements conducted in paper III were the first measurements of optical emission spectra from industrial AC EAF, and provided a new insight on the EAF arc plasma. The optical emission spectra of laboratory, pilot and industrial EAFs are shown in Figure 13. The similarities of the three spectra obvious, the largest difference is that the lines are slightly broader in the spectrum from pilot EAF. This can be attributed to different spectrometer used in the pilot measurements.

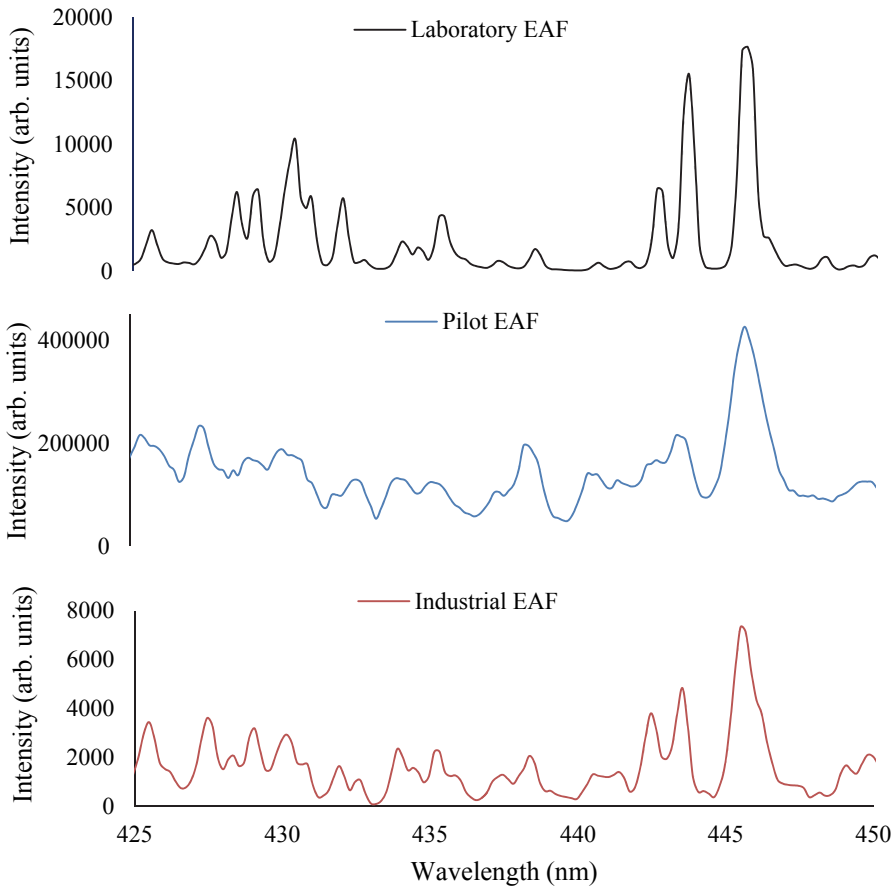


Fig. 13. Optical emission spectrum of laboratory, pilot and industrial EAF.

Measurements on industrial and pilot furnaces show that in naked arc conditions the emitting components in the plasma mainly originate from the slag. Most of the measured lines are related to Ca I, Cr I, Mg I, Mn I or Fe I. Atomic emission lines of alkali metals are also observed. The atoms originating from slag components enter the arc plasma when the high temperature of the electric arc vaporizes and decomposes the slag components.

The presence of other atoms besides iron in arc plasma indicates that the accuracy of plasma heat transfer models could be improved by implementing net

emission coefficients of other atomic species. A substantial amount of the heat of the arc is emitted from the transitions of Ca I, Cr I, Mn I and atomic emissions of alkali metals. The presence of different atoms in arc plasma can have a significant effect on plasma temperature since the energy of plasma is dissipated by atomic line emissions. It has been demonstrated that when the amount of iron in plasma increases, the plasma column is substantially cooled due to increased radiative energy loss [71]. The cooling effect of different slag components depends on intensity and amount of their optical emission lines. The cooling effect is increased by the endothermic vaporization and decomposition of slag components in the edges of the arc.

In addition, the composition of arc plasma has a significant effect on the optical thickness of the plasma. Since the line radiation has been previously assumed to be mostly emitted by iron, only the optical thickness of Fe I lines has been studied. In measurements conducted in Paper III, the Ca I lines emitted from the arc plasma have been defined as optically thin when the electron temperature is below 7000 K. The low optical thickness was defined from the accuracy of the Boltzmann plot. An example of the effect of increasing plasma temperature on the accuracy of the Boltzmann plot is presented in Figure 14.

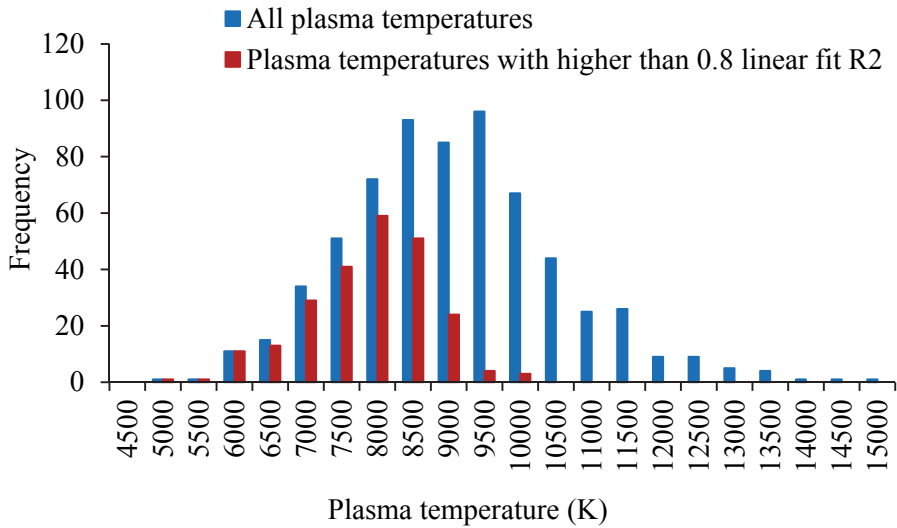


Fig. 14. Histogram of all plasma temperatures and accurate plasma temperatures for an example heat calculated from Ca I lines [Paper III, reprinted by permission of Metallurgical and Materials Transactions B].

6.2 EAF slag composition

EAF slag composition was analysed from the relative intensities of different atomic components in the arc emission spectra. The focus of the analysis was in the CrOx content of the slag because it affects the amount of solid chromium containing precipitates in slag and influences the reduction of chromium in tapping [20].

6.2.1 Feasibility of analysing slag composition ratios with fluctuating arc length

The first requirement of using the optical emission spectrum in EAF slag composition analysis is that the atoms and ions in the arc plasma originate from the slag. This assumption is valid in industrial EAFs, as discussed earlier chapter in 5. The main difficulty in measuring the EAF slag composition is that the position of the electric arc is in constant change. The optical emission of the arc obtained from EAF will describe different parts of the arc plasma. As the electron temperature of

the plasma changes, the number density and probability of atomic excitation will change.

The feasibility of analysing slag composition from optical emission of fluctuating electric arc was studied by measuring optical emission spectra of industrial slag samples in the laboratory furnace described in chapter 5.1. These measurements were reported in Paper I. The arc length was varied by changing the distance of the electrodes by manually. The results were analysed by calculating the Pearson product momentum correlation between all combinations of peak ratios between 251 measured optical emission lines to the slag composition ratios.

The results of the correlation analysis showed that every line ratio with high correlation to slag composition ratio contains either slag components Cr_2O_3 or MnO . The correlation analysis was verified by comparing the optical emission lines with high correlations to the NIST documented line positions [72]. NIST verification indicates that due to high correlation between Cr_2O_3 and MnO , Cr I lines and Mn I lines were somewhat mixed in the correlation analysis.

Cr_2O_3 and MnO being in every line ratio with high correlation to slag composition indicates that fluctuation of these components are the most accurately described by the optical emission spectrum. $\text{Cr}_2\text{O}_3/\text{FeO}$ ratio could be approximated with relative error between 11 and 14% depending on the arc voltage and had linear regression of 0.95 – 0.96 to slag composition. The results showed that measuring the change in relative content Cr_2O_3 and MnO in slag from arc optical emission spectrum is feasible on the laboratory scale.

6.2.2 Accuracy of analysing slag CrO_x content

As good results of analysing slag CrO_x content were obtained from laboratory EAF, further measurements on the accuracy of measuring CrO_x content were conducted with the pilot scale EAF. In the pilot EAF, the furnace configuration resembles industrial EAF better and slag is more inhomogeneous than in the laboratory furnace. The details of the pilot furnace and the test practice were presented in chapter 5.2 and reported in Paper II. The Cr_2O_3 content of the slag was gradually increased with Cr_2O_3 powder additions and the measured emission spectra were compared to the slag composition measured with XRF analysis.

The highest linear regression R^2 values for different component ratios in laboratory and pilot measurements are presented in Table 11. The results are in line with the laboratory measurements, the highest linear regressions to slag composition ratios were obtained for line ratios Cr I/Ca I, Cr I/Fe I and C I/Mn I.

The highest linear regression R^2 values were lower than in laboratory measurements; slag $\text{Cr}_2\text{O}_3/\text{FeO}$ could be approximately with linear regression R^2 of 0.95 in laboratory measurements.

Table 11. Linear regression between the line ratios and the respective slag composition ratios [modified from Paper II].

Reference	–	Mg I	Ca I	Fe I	Mn I
The highest R^2	0.61	0.74	0.85	0.84	0.86
Average of five highest R^2	0.59	0.74	0.83	0.78	0.80
Count of over 0.75 R^2	0	0	8	3	12

The slag Cr_2O_3 content was analysed by combining the line ratios of Cr I/Ca I, Cr I/Fe I and C I/Mn I. The analysis relies on the line ratios being dominated by changes in slag Cr_2O_3 content. The ratios were first modified to relative form by dividing them with maximum of the line ratio and then combined by calculating mean of relative line ratios. With the mean of relative line ratios, the slag Cr_2O_3 content could be approximated with an average absolute error of 0.62%-points and standard deviation of 0.49%-points. The median of relative line ratios and median absolute deviation from median (MAD) are presented in Figure 15. MAD was selected as a description of variability instead of standard deviation because it represents data with outliers better than standard deviation.

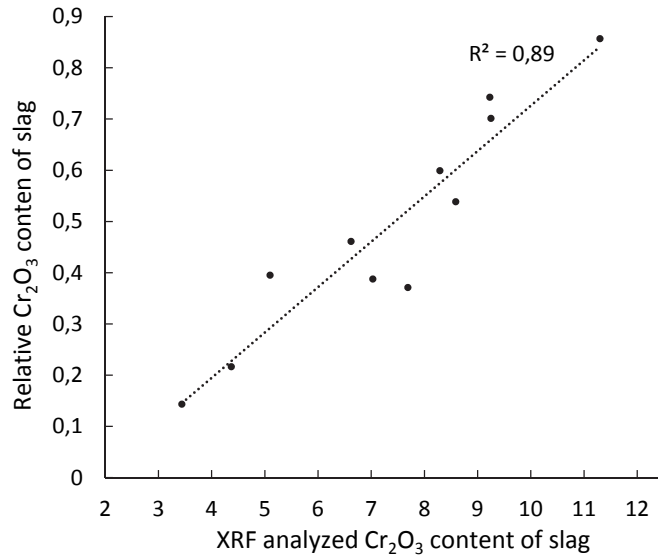


Fig. 15. Linear approximation of slag Cr₂O₃ content with average of relative line ratios [modified from Paper II].

6.3 EAF process conditions

The connections between industrial EAF emission spectrum and EAF process conditions was studied in Papers III and IV. The optical emission spectra measured from EAF can be divided to four different categories presented in Figure 16.

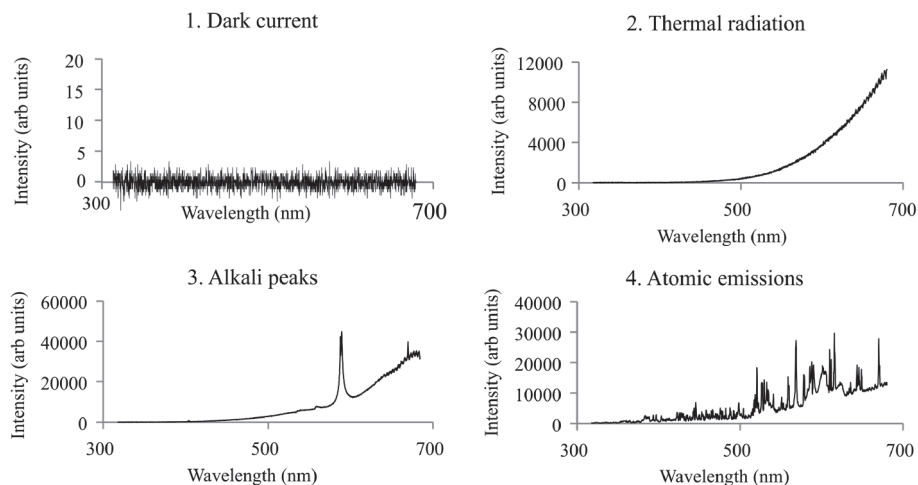


Fig. 16. Different types of spectra observed in industrial EAF [Paper III, reprinted by permission of Metallurgical and Materials Transactions B].

The analysis of process conditions mainly focused on analysing the spectrum types dominated by dark current, thermal radiation and alkali transitions. These three types of spectra can be used in analysing gas phase reactions, as well as surface conditions of slag and steel scrap. The arc emission spectra were not compared to process conditions because arc emission spectra was measured only for a low amount of heats due to changes in arc position and visibility. According to the results presented in Paper IV, the behaviour of emission spectra varies between different process periods. By analysing the evolution of spectrum indicators during different process periods, the optical emission spectra were found to relate to the volatilization of scrap contaminants, scrap melting, arc voltage set-point, momentary high CO generation and changes in characteristics of the slag surface. The occurrence of these phenomena during an example heat is presented in Figure 17.

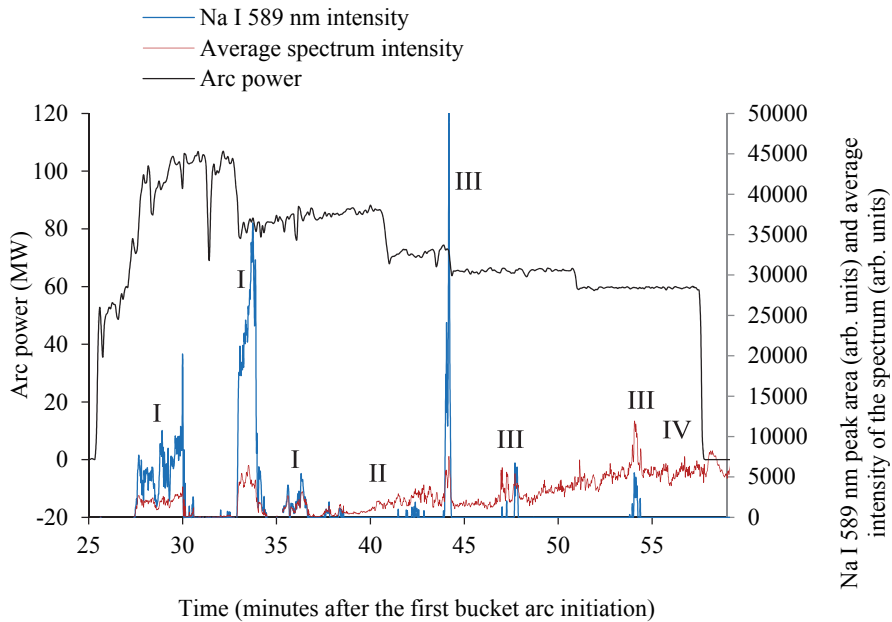


Fig. 17. Occurrence of the studied phenomena during an example heat (I. Volatilization of scrap contaminants II. Scrap melting III. Spontaneous CO generation IV. Slag surface conditions) [Paper IV, reprinted by permission of ISIJ International].

6.3.1 Volatilization of scrap contaminants

During early process periods, optical emission spectra with a high spectrum temperature can be observed. These high temperature emission spectra can appear and disappear in the course of minutes or last for a good part of the early melting periods. The early occurrence, high spectrum temperature and high average intensity suggest that these emission spectra are related to the combustion of volatile gases in the EAF. The correlation can be verified from visual observations of flames escaping the EAF. These flames are also related to the intensity of alkali emission lines in the spectra. During early process periods, the optical thickness of EAF atmosphere is very high, which means that not all combustion occurring in the EAF atmosphere can be observed in the emission spectra.

6.3.2 Spontaneous generation of CO

When scrap melts in the EAF, the combustion of volatile components decreases and high spectrum temperatures and the intensity of alkali emission lines are related to the CO generation occurring in the EAF. The connection between sodium 589 nm line intensity and off-gas composition is presented in Figure 18. The spontaneous CO generation is not limited to melting periods of EAF, but happens also in the heating period.

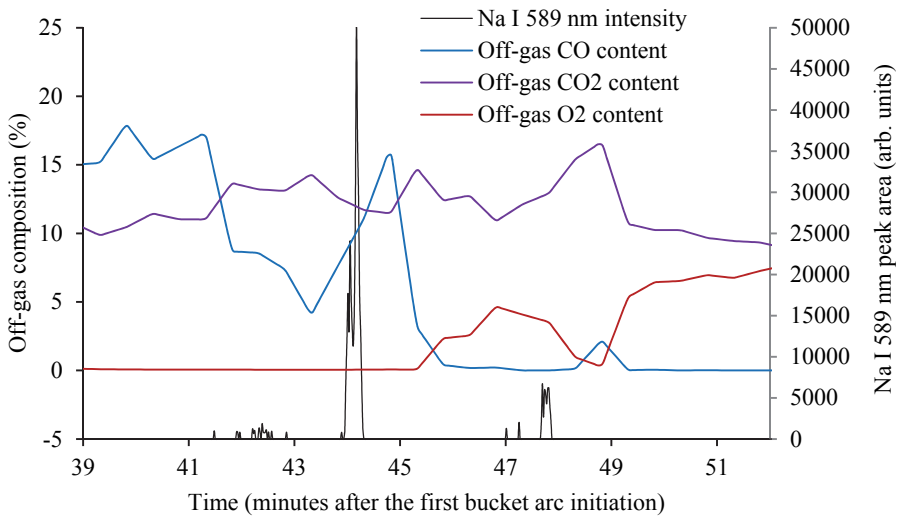


Fig. 18. Intensity of Na I line and off-gas mass spectrometry (MS) analysis [Paper IV, reprinted by permission of ISIJ International].

The increase in CO generation is most likely caused by a combination of initial generation of CO and increased mixing due to generation of CO bubbles. The reactions between slag and steel are limited by mass transfer in slag due to high viscosity of CrO_x containing slag, which causes concentration gradients in the slag. High CO generation can cause momentary foaming or introduce steel droplets to slag, which can increase the mass transfer in slag and interfacial area between steel and slag. The increased reaction area and mass transfer cause more intense oxidation-reactions, which further promote the generation of CO.

Initially, CO is generated when the solid scrap accumulated on the furnace sides collapses into the steel melt. This introduces oxidic contaminants of the scrap

to the steel melt and increases mixing between steel and slag. The effect of increased mixing on CO generation depends on the inhomogeneity of the steel melt and slag, as well as deviation from the thermodynamic equilibrium between steel and slag. However, it is not clear if the spontaneous CO generation actually requires scrap collapse with high enough slag inhomogeneity. In the main melting period, scrap collapses are more frequent and their effect is probably more pronounced. Material can also fall from the sides when the furnace is tilted in EAF tapping.

6.3.3 Scrap melting

During early EAF process periods, the cold scrap obstructs the view to the furnace. When the scrap in the viewing cone starts to melt, the hot scrap near the slag starts to appear under the solid scrap layer and the intensity of the light emitted from the measured area increases. However, the combustion of volatile gases can also increase the intensity of the optical emission spectrum, which means that the effect of flames must be removed in order to gain accurate information on scrap melting.

The analysis of scrap melting in Paper IV is simplified by the lack of burner flames during the measurement period, which means that the flames affecting the measured spectra originate from the volatile components and generation of CO. The flames caused by volatile components and CO generation can be removed by analysing the intensity of the alkali transitions and the temperature of the optical emission spectra. As discussed earlier, the flames increase spectrum temperature and are related to the high intensity of alkali optical emission lines.

By defining an indicator for scrap melting and removing the effect of flames it is possible to analyse the timing of scrap melting in different heats. In Paper IV the scrap melting was deemed to have progressed to a certain stage when the average intensity of the 60 last frames first increases over 600 counts. The effect of flames was removed by setting a criterion of spectrum temperature being below 1600 C and the linear fit of last 10 frames of spectrum temperature being positive. The value of scrap melting indicator is arbitrary, as it is not certain how the indicator is related to the specific stage of scrap melting. The purpose of the indicator is to provide a tool for analysing relative changes in melting during different heats.

The variation in the scrap melting during different heats can be compared by calculating the time when the optical emission spectrum meets the scrap melting criterion. A better description of the state of the EAF process can be obtained when time is replaced with the energy inserted to the EAF. This removes the effect of changing voltage set-points. The ratio of energy inserted after the scrap melting

criterion is fulfilled to the total inserted energy is presented in Figure 19. It can be observed in that most of the heats have the ratio in range of 0.2 to 0.5. In some cases the scrap melting is observed much later, approximately 27% of the heats have over 0.5 of the energy inserted in flat bath conditions. The results indicate that there is significant variation in the scrap melting during different heats.

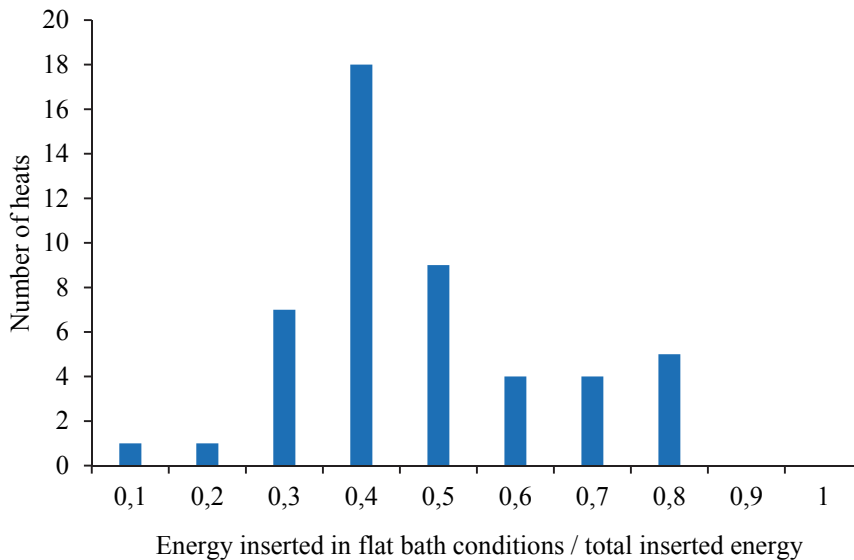


Fig. 19. Histogram of ratios between inserted energy in flat bath conditions and total inserted energy [Paper IV, reprinted by permission of ISIJ International].

6.3.4 Slag surface conditions

The changes in energy input are reflected in spectrum indicators. The decrease of voltage ramp decrease the spectrum intensity and temperature measured from electrode hot-spot. In some rare cases it can also have had a reverse effect on the spectrum temperature. The decrease of spectrum temperature can be explained by decrease of arc length in arc voltage change. The heat transfer between slag surface and the electric arc is significantly affected by arc length. Sanchez et al [73] demonstrated that when the electrode is over 11.25 cm over the slag surface rather than 22.5 cm, it reduced average incident radiation on the slag surface by 12.5%.

As emissivity (and absorptivity) of slag can be as high as 0.9 [74]), the incident radiation results in increased slag surface temperature.

Spectrum temperature is also observed to change during the heating period when the arc voltage set-point is constant. The trend in 70% of the measured heats was towards higher temperatures, which suggests that the increase in steel melt temperature in the heating period has some effect on slag surface temperature. An example of slag surface temperature evolution during the heating period of the EAF process is presented in Figure 20. On the other hand, the effect is not always straightforward, as in 9% of the measured heats the trend of decreasing slag surface conditions can be observed. In 51% of the measured heats there is no clear temperature trend or the length of the heating period is not long enough to analyse long-term trends. Nevertheless, it seems that especially in the heating period, the optical emission spectrum is related to the surface temperature and possibly to emissivity of slag.

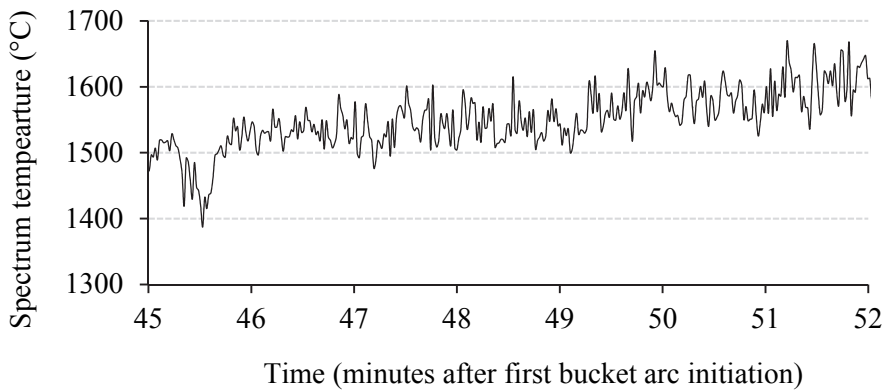


Fig. 20. An example of temperature evolution during a heating period [Paper IV, reprinted by permission of ISIJ International].

7 Industrial relevance

The most promising potential uses of emission spectrum measurement in monitoring of industrial stainless steelmaking EAFs are slag composition analysis and analysis of scrap melting. In addition, the results can be used to make more valid assumptions in EAF heat transfer modelling.

7.1 Slag composition calculated from arc emission spectrum

As demonstrated in paper III, most of the atomic emission lines originate from the components of the slag. This indicates that there is a connection between EAF slag composition and arc emission spectrum. In the laboratory and pilot furnace measurements promising results were obtained for analysis of CrO_x/FeO and CrO_x/MnO ratios of the slag. With selection of a narrower spectral band, it could be possible to increase the accuracy and analyse also other slag components.

The CrO_x/MnO and CrO_x/FeO ratios of the slag could be used in mitigation of slag CrO_x content. Because the amounts of CrO_x , MnO and FeO are influenced by the oxidation–reduction reactions in the furnace, the levels of CrO_x , MnO and FeO in slag are linked. This correlation reduces the effect of other process parameters e.g. slag amount and charge composition on the CrO_x/MnO and CrO_x/FeO ratios. The connection between slag CrO_x , MnO and FeO also causes the ratios of CrO_x/MnO and CrO_x/FeO to mainly reflect the changes in oxidation conditions, which in turn means that these component ratios can be used to assess how far the CrO_x oxidation has progressed and evaluate what is the level of CrO_x in the slag.

In pilot EAF measurements the accuracy of measuring slag CrO_x content could be increased by combining multiple component ratios. The average absolute error of 0.62%-points in slag CrO_x content analysis would be acceptable in industrial EAF considering there is currently no information of slag CrO_x content. The slag samples taken from an industrial EAF showed that the level of slag Cr_2O_3 content in that EAF varied between 7 and 14 wt-% [22], which means that the variation of slag Cr_2O_3 content is significantly higher than the average absolute error level in pilot measurements.

The analysis of CrO_x in the EAF slag would allow mitigation of ladle slag CrO_x content. The high CrO_x content in EAF slag indicates high ladle CrO_x because high CrO_x increases the amount of chromium containing precipitates, which have high incubation time for chromium reduction. If the high CrO_x content of the slag is measured early enough, it would be possible to make necessary additions of

reducing agents to steel to promote the CrO_x reduction in the heating period and tapping, or promote slag mixing with various stirring methods.

Another way to use information on slag high CrO_x content would be to process the high CrO_x slag in a different way after the tapping compared to normal slag. One method would be to introduce reducing agents straight to the slag ladle. In addition, the increased viscosity of slag with high CrO_x content increases the residence times of metal droplets in slag, which means that slag with high CrO_x content has higher amount of metal droplets in it. Therefore, slag with high CrO_x would require more efficient recovery of metals trapped in the slag matrix.

7.2 Average scrap melting

One of the most promising future applications of optical emission spectrometry is the analysis of local scrap melting. Currently, the methods to measure scrap melting are very limited, although the local scrap melting conditions have a substantial effect on arc efficiency and charging practice of EAF. Currently, the state of the art method to analyse local scrap melting conditions is to measure energy loss to water-cooled side panels. However, the temperature increase in side panel cooling water has a delay depending on the thickness of slag layer on the furnace side panels. Reliable on-line scrap melting analysis would provide a method to compensate the changes in scrap melting between different heats.

The signal of scrap melting would make it possible to optimize the scrap buckets to reduce the variation in scrap volume inside the furnace after charging. This could be achieved by defining the evolution of local scrap melting and by using it to assess how large free volume there is in furnace. Better control of charging would reduce under- and overcharging. Overcharging can cause significant delay in the EAF process while undercharging loses process time and energy due to input of energy due to early occurrence of flat bath conditions.

During the melting periods the combustion of the scrap contaminants is often observed in the emission spectrum. In analysis of local scrap melting the largest challenge is how to differentiate between the emission spectrum being emitted by the flames or by hot slag appearing in the view. The conditions can be differentiated by some degree with spectrum diagnostics, but the most accurate expression of scrap melting can be obtained by combining the emission spectrum measurement with other measurements less affected by combustion of contaminants, namely the electrode position and cooling water energy increase.

7.3 Optimization of arc voltage

The local scrap melting signal would be beneficial in control of arc voltage in stainless steelmaking EAF. When scrap in an electrode hot-spot is melted, the energy efficiency of the arc is decreases. This should be compensated by decrease in arc length to reduce the view factor between arc and refractories. On the other hand, if the melting in a certain electrode hot-spot is observed later than normal, the high electrode voltage could be maintained longer. The advantages of local scrap melting signal depends on the fact that the modification of voltage of single electrode is possible in furnace in question.

The use of optical emission spectrum in arc voltage optimization would require information of local scrap melting conditions, which could be acquired by using multiple optical fibres and measurement heads. While the furnace charging optimization requires information of scrap melting averaged over whole furnace, the energy efficiency of a single electrode depends on the local scrap melting conditions. It is not certain how uniform the scrap melting is near different electrodes.

The connection between arc voltage changes and spectrum temperature suggests that emission spectrum measurement can be also used in analysis of heat transfer from slag surface to refractories. High spectrum intensity and temperature with constant arc voltage suggests that the difference between slag height and electrode tip is high and arc length should be reduced. The optimal use of the slag surface heat transfer analysis would require defining a certain threshold for emission intensity, over which the refractory wear becomes too high. The threshold depends on the requirement of furnace productivity. If the EAF is the bottleneck of the process, as usually is the case in stainless steelmaking, the threshold should be set so high that it the system reacts only when the refractory wear is unacceptable.

In the production of carbon steel grades, the scrap melting signal could be used in assessment of slag foaming. If the scrap melts early, the carbon injection could be also started earlier. The first measurements in carbon steelmaking EAF [75], suggests that with optimized carbon injection significant increase in energy efficiency could be obtained.

7.4 Assumptions of EAF heat transfer models

The results reported in this work can be used to validate the assumptions of EAF heat transfer models. The observation of atomic components originating from the slag in the arc plasma suggests that the accuracy of plasma models only considering iron vapour in plasma could be improved. The measurement of optically thin plasma emission spectrum in heating period suggests that in later periods of EAF processing, the EAF atmosphere can be optically thin, which means that the radiation from the arc can reach the furnace sides unchanged. This highlights the importance of considering the radiation from the arc plasma generated by the atomic emissions. In order to gain a more accurate description of arc heat transfer, further measurements of the composition of industrial EAF arc plasma are required.

7.5 Implications for the development in the future

From perspective of novelty, the most interesting finding of this dissertation is that the slag chromium composition can be estimated from the optical emission spectrum of the electric arc. As the CrO_x analysis of stainless steelmaking slags have been tested in laboratory and pilot furnaces, the emphasis in further development should be on the implementation of these methods in industrial furnaces. In case of carbon steelmaking, more information on the arc emission spectrum is still required. In its implementation in the industrial EAF, the most important aspects are how to acquire high quality optical emission spectra of the electric arc continuously and to evaluate the effect of inhomogeneity of the slag to the measurement results. Also, using the measurement system in routine process control requires the availability of the measurements system to be enhanced, especially concerning the accumulation of slag in the measurement hole. Industrial trials on slag composition measurement are being planned as this dissertation is being published.

Concerning the scrap melting and slag surface conditions, industrial applications are already on the horizon. To obtain accurate information of EAF process conditions, the data from optical emission spectrum measurement should be combined to other on-line process data on the EAF. Optical emission spectrum measurement would complement the scrap melting data obtained from water-cooled copper panel temperatures, as there is the problem of delay.

8 Summary

The aim of the thesis was to use optical emission spectrometry to analyse EAF arc plasma characteristics, slag composition and process conditions. Optical emission spectra from laboratory, pilot and industrial scale furnaces were measured and analysed.

The analysis of atomic emission lines in optical emission spectra indicate that the arc plasma in an industrial EAF contains atoms originating from the vaporization of slag. The results show the accuracy of EAF heat transfer models could be increased by employing net emission coefficients of these atoms. The atoms in EAF arc plasma originating from the slag indicates that slag composition can affect arc composition. Electron temperature calculations of measured emission spectra show that Ca I lines used in Boltzmann plot are optically thin to 7000 K. The low scatter in Boltzmann plots calculated from the measured optical emission spectra indicate that in the late periods of EAF processing the optical emissions from can reach furnace sides without undergoing absorption.

Slag composition was analysed by measuring the optical emission spectrum of electric arc in the laboratory and pilot scale furnaces. The laboratory analysis shows that composition ratios of MnO and CrO_x can be measured most accurately. Analysing the CrO_x content of the slag was further studied by conducting measurements on the arc emission spectrum of the pilot scale furnace. By combining composition ratios of multiple components it was possible to estimate the Cr₂O₃ content of the slag with average absolute error of 0.62%-points.

The optical emission spectrum measured from industrial EAF was found to relate to the EAF process conditions. Combustion of volatile components in the scrap charge and generation of CO was found to correlate to spectrum temperature and the intensity of alkali emission lines. The optical emission spectrum was also found to be affected by the melting of the scrap and surface conditions of the slag in late process periods.

The results indicate that the method could be used in process control for analysing scrap melting and the amount of CrO_x in slag. However, industrial trials of CrO_x analysis are still required. Accurate determination of local scrap melting in stainless steelmaking EAF allows better control of arc voltage, which can increase productivity and decrease refractory wear. Analysing CrO_x content of the slag allows the optimization of reducing agent additions and mixing to reduce the amount of CrO_x in slag after EAF tapping.

References

1. Toulevski YN & Zinurov IY (2010) Innovation in Electric Arc Furnaces – Scientific Basis for Selection. Heidelberg, Springer.
2. Gebhart B (ed) (1971) Heat Transfer. McGraw-Hill.
3. Konuk AR, Aarts RGKM, Huis in 't Veldt AJ, Sibillano T, Rizzi D & Ancona A (2011) Process Control of Stainless Steel Laser Welding Using an Optical Spectroscopy Sensor. *Physics Procedia* 12 (Part A): 744–751.
4. Mauer G, Guignard A, Vaßen R & Stöver D (2010) Process diagnostics in suspension plasma spraying. *Surface & Coatings Technology* 205: 961–966.
5. Song L & Mazumder J (2012) Real Time Cr Measurement Using Optical Emission Spectroscopy During Direct Metal Deposition Process. *IEEE Sensors Journal* 12(5): 958–964.
6. Rego-Barcena S, Mani R, Yang F, Saari R & Thomson MJ (2009) Real-Time, Optical Measurement of Gas Temperature and Particle Emissivity in a Full-Scale Steelmaking Furnace. *Metallurgical and Materials Transactions B* 40B(4): 158–168.
7. Chiba K, Ono A, Saeki M, Yamauchi M, Kanamoto M & Ohno T (1993) Development of Direct Analysis Method for Molten Iron in Converter: Hotspot Radiation Spectrometry. *Ironmaking & Steelmaking* 20(3): 215–220.
8. Veillette P & Simard D (1984) Electric Arc Characterization Using High Speed Cinematography and Spectroscopy. Electric furnace conference. Toronto, Iron and Steel Society: 173–182.
9. Block O (1995) Spektroskopische Untersuchungen von frei brennenden Gleichstromlichtbogen mit hoher Leistung an einem Elektrostahlofen. University of the Federal Armed Forces, Hamburg.
10. Boyd TJM & Sanderson JJ (2003) *The Physics of Plasmas*. Cambridge, UK, Cambridge University Press.
11. Aragón C & Aguilera JA (2008) Characterization of laser induced plasmas by optical emission spectroscopy: A review of experiments and methods. *Spectrochimica Acta Part B* 63: 893–916.
12. Griem HR (1964) *Plasma Spectroscopy*. New York, McGraw-Hill.
13. Ovsyannikov AA & Zhukov MF (2000) *Plasma diagnostics*. Cambridge, GBR, Cambridge international science publishing.
14. Jones JAT, Bowman B & Lefrank PA (1998) Electric Furnace Steelmaking. In: Fruehan RJ (ed). *The Making, Shaping and Treating of Steel, Steelmaking and Refining Volume*. Pittsburgh. AISE Steel Foundation: 525–660.
15. Bowman B & Krüger K (2009) *Arc Furnace Physics*. Düsseldorf, Germany. Verlag Stahleisen GmbH.
16. Guo M, Durinck D, Jones PT, Heylen G, Hendrickx R, Baeten R, Blanpain B & Wollants P (2007) EAF Stainless Steel Refining - Part I: Observational Study on Chromium Recovery in an Eccentric Bottom Tapping Furnace and a Spout Tapping Furnace. *Steel Research International* 78(2): 117–124.

17. Matsuura H & Fruehan RJ (2006) Slag Foaming in an Electric Arc Furnace. *ISIJ International* 49(10): 1530–1535.
18. Ito K & Fruehan RJ (1989) Study on the foaming of CaO-SiO₂-FeO slags: Part I. Foaming parameters and experimental results. *Metallurgical and Materials Transactions B* 20(4): 509–514.
19. Kerr JJ & Fruehan RJ (2004) Additions to Generate Foam in Stainless Steelmaking. *Metallurgical and Materials Transactions B* 35B(4): 643–650.
20. Görnerup M & Lahiri AK (1998) Reduction of electric arc furnace slags in stainless steelmaking: Part I Observations. *Ironmaking & Steelmaking* 25(4): 317–322.
21. Kerr JJ & Fruehan RJ (2002) Foamability of Stainless Steelmaking Slags in an EAF. *Iron & Steelmaker* 29(4): 45–52.
22. Durinck D, Jones PT, Guo M, Verhaeghe F, Heylen G, Hendrickx R, Baeten R, Blanpain B & Wollants P (2007) EAF Stainless Steel Refining - Part II: Microstructural Slag Evolution and its Implications for Slag Foaming and Chromium Recovery. *Steel Research International* 78(2): 125–135.
23. Huck M (2012) Boosting Profitability with Siemens VAI EAF Modernization. 10th European Electric Arc Furnace Conference. Graz, Austria. ASMET.
24. Mees H (2012) Chromverschlackung bei der Erzeugung von chromhaltigen Schmelzen im Elektrolichtbogenofen und die Möglichkeiten zu deren Verringerung. RWTH Aachen.
25. Kleimt B, Nyssen P, Mathy C, Weber M, Borlée J, Simon P, Baumert JC, Landa S, Kühn R & Deng J (2007) Dynamic control of EAF burners and injectors for carbon and oxygen for improved and reproducible furnace operation and slag foaming. EUR 23920.
26. Kühn R, Geck HG & Schwerdtfeger K (2005) Continuous Off-gas Measurement and Energy Balance in Electric Arc Steelmaking. *ISIJ International* 45(11): 1587–1596.
27. Wu Q, Thomson MJ & Chanda A (2005) Tunable Diode Laser Measurements of CO, H₂O, and Temperature Near 1.56 μm for Steelmaking Furnace Pollution Control and Energy Efficiency. *Metallurgical Materials Trans B* 36B(2): 53–57.
28. Risonarta VY, Echterhof T, Jung HP, Beiler C, Lenz S, Kirschen M & Pfeifer H (2010) Application of an Off-Gas Analysing System to Control Oxidation during Stainless Steelmaking in an EAF. *Steel Research International* 81(9): 778–783.
29. Mees H, Höhl J, Krüger K, Rieger D, Matschullat T, Döbbeler A & Dittmer B (2012) Dynamic Condition Based Scrap Melt Control: Results of the Application at Thyssenkrupp Nirosta in Bochum. 10th European Electric Arc Furnace Conference. Graz, Austria. ASMET.
30. Jansen T, Krüger K, Schliephake H, Dettmer B & Schlinge L (2012) Advanced Foaming Slag Control. 10th European Electric Arc Furnace Conference. Graz, Austria. ASMET.
31. Grygorov P, Jepsen O, Odenthal H-J, Reifferscheid M & Theobald F (2012) Computer modeling and Experimental Validation of an Electric Arc Furnace. 10th European Electric Arc Furnace Conference. Graz, Austria. ASMET.
32. Lin L & Mao Z (2012) A direct adaptive controller for EAF electrode regulator system using neural networks. *Neurocomputing* 82: 91–98.

33. Sheshukov OY, Nekrasov IV, Sivtsov AV, Tsymba MM, Egiazar'yan DK & Metelkin AA (2014) Dynamic monitoring of slag oxidation and thickness in the ladle-furnace unit. *Steel in Translation* 44(1): 43–46.
34. Edwards DK (1981) *Radiation Heat Transfer Notes*. Washington DC. Hemisphere publishing.
35. Reynolds Q (2002) Thermal radiation modelling of DC smelting furnace freeboards. *Minerals Engineering* 15: 993–1000.
36. Orhan G (2005) Leaching and cementation of heavy metals from electric arc furnace dust in alkaline medium. *Hydrometallurgy* 78(3-4): 236–245.
37. Dutra AJB, Paiva PRP & Tavares LM (2006) Alkaline leaching of zinc from electric arc furnace steel dust. *Minerals Engineering* 19(5): 478–485.
38. Nyirenda RL (1991) The processing of steelmaking flue-dust: A review. *Minerals Engineering* 4(7-11): 1003–1025.
39. Caravaca C, Cobo A & Alguacil FJ (1994) Considerations about the recycling of EAF flue dusts as source for the recovery of valuable metals by hydrometallurgical processes. *Resources, Conservation and Recycling* 10(1-2): 35–41.
40. Ma G & Garbers-Craig AM (2006) A review on the characteristics, formation mechanisms and treatment processes of Cr (VI)-containing pyrometallurgical wastes. *The Journal of The Southern African Institute of Mining and Metallurgy* 106: 753–763.
41. Stefanova A & Aromaa J (2012) Alkaline leaching of iron and steelmaking dust. Aalto University publication series SCIENCE + TECHNOLOGY, 1/2012.
42. Ruiz O, Clemente C, Alonso M & Alguacil FJ (2007) Recycling of an electric arc furnace flue dust to obtain high grade ZnO. *Journal of Hazardous Material* 141: 33–36.
43. Youcai Z, Stanforth R (2000) Integrated hydrometallurgical process for production of zinc from electric arc furnace dust in alkaline medium. *Journal of Hazardous Material* 80(1-3): 223–240.
44. Xia DK & Pickles CA (1999) Caustic roasting and leaching of electric arc furnace dust. *Canadian Metallurgical Quarterly* 38(3): 175–186.
45. Jarupisitthorn C, Pimtong T & Longhongkum G (2002) Investigation of kinetics of zinc leaching from electric arc furnace dust by sodium hydroxide. *Material Chemistry and Physics* 77(2): 531–532.
46. Dreisinger DB, Peters E & Morgan G (1990) The hydrometallurgical treatment of carbon steel electric arc furnace dusts by the UBC-Chaparral process. *Hydrometallurgy* 25(2): 137–152.
47. Guézennec AG, Huber JC, Patisson F, Sessiecq P, Birat JP & Ablitzer D (2005) Dust formation in electric arc furnace: Birth of the particles. *Powder Technology* 157: 2–11.
48. Paik S & Nguyen HD (1995) Numerical modeling of multiphase plasma/soil flow and heat transfer in an electric arc furnace. *International Journal of Heat and Mass Transfer* 38(7): 1161–1171.
49. Logar V & Škrjanc I (2012) Modeling and Validation of the Radiative Heat Transfer in an Electric Arc Furnace. *ISIJ International* 52(7): 1225–1232.
50. MacRosty RDM & Swartz CLE (2005) Dynamic Modeling of an Industrial Electric Arc Furnace. *Industrial & Engineering Chemistry Research* 44: 8067–8083.

51. Millman M, Nyssen P, Mathy C, Tolazzi D, Londero L, Candusso C, Baumert JC, Brimmeyer M, Gualtieri D & Rigoni D (2008) Direct observation of the melting process in an EAF with a closed slag door. *Archives of Metallurgy and Materials* 53(2): 463–468.
52. Jones RT, Reynolds QG & Alport MJ (2002) DC arc photography and modelling. *Minerals Engineering* 15(11): 985–991.
53. Haidar J (1998) A theoretical model for gas metal arc welding and gas tungsten arc welding. I. *Journal of Applied Physics* 84: 3518–3529.
54. Bakken JA, Gu L, Larsen HL & Sevastyanenko VG (1997) Numerical Modeling of Electric Arcs. *Journal of Engineering Physics and Thermophysics* 70(4): 530–543.
55. Ramírez M & Trapaga G (2004) Mathematical modeling of a direct current electric arc: Part I. Analysis of the characteristics of a direct current arc. *Metallurgical and Materials Transactions B* 35(2): 363–372.
56. van der Sijde B & van der Mullen JAM (1990) Temperature determination in non-LTE plasmas. *Journal of Quantitative Spectroscopy and Radiative Transfer* 44(1): 39–46.
57. Wang F, Jin Z & Zhu Z (2006) Numerical study of dc arc plasma and molten bath in dc electric arc furnace. *Ironmaking and Steelmaking* 33(1): 39–44.
58. Qian F, Farouk B & Muthasaran R (1995) Modeling of Fluid Flow and Heat Transfer in the Plasma Region of the dc Electric Arc Furnace. *Metallurgical and Materials Transactions B* 26B(10): 1057–1067.
59. Alexis J, Ramirez M, Trapaga G & Jönsson P (2000) Modeling of a DC Electric Arc Furnace - Heat Transfer from the Arc. *ISIJ International* 40(11): 1089–1097.
60. Ramírez-Argaéz MA, González-Rivera C & Trápaga G (2009) Mathematical Modeling of High Intensity Electric Arcs Burning in Different Atmospheres. *ISIJ International* 49(6): 796–803.
61. Kiyoumarsı A, Nazari A, Ataei M, Beheshti HK & Hooshmand R-A (2010) Electromagnetic analysis of an AC electric arc furnace including the modeling of an AC arc. *The International Journal for Computation and Mathematics in Electrical and Electronic Engineering* 29(3): 667–685.
62. Bowman B (2012) Broad, Radiation-Dominated Arcs in Steel and Ferroalloy Furnaces. 10th European Electric Arc Furnace Conference. Graz, Austria. ASMET.
63. Ramírez-Argaéz MA, González-Rivera C & Trápaga G (2009) Mathematical Modeling of High Intensity Electric Arcs Burning in Different Atmospheres. *ISIJ International* 49(6): 796–803.
64. Hergt M, Hartmann W & Matschullat T (2015) Influence of poly atomic gases on physical properties of the EAF arc plasma. Proceedings of the 2. European Steel Technology and Application Days (ESTAD). Düsseldorf, Germany. The Steel Institute VDeh.
65. Saevarsdottir GA, Bakken JA (1998) Radiative transfer in industrial thermal plasmas of complex composition. *Progress in Plasma Processing of Materials 1999: Proceedings of the Fifth International Thermal Plasma Processes Conference*, St. Petersburg. New York. Begell House.

66. Saevarsdottir GA, Bakken JA, Sevastyanenko VG, Gu L (2001) Arc Simulation Model for Three-Phase Electro-Metallurgical Furnaces, INFACON 9. Quebec City, Canada. The Ferroalloys Association.
67. Mäkinen A (2013) Experimental Spectroscopic Studies of Metals with Electron, Ion and Optical Techniques. Report Series in Physical Sciences No. 87. University of Oulu.
68. Dereniak EL & Crowe DG (1984) Optical Radiation Detectors. New York, John Wiley & Sons.
69. Brun R & Rademakers F (1997) ROOT - An Object Oriented Data Analysis Framework. Nuclear Instruments and Methods in Physical Research. A 389: 81–86.
70. Anon (2009) Teräskirja. Tampere, Finland, Metallinjalostajat ry.
71. Gonzalez JJ, Gleizes A, Proulx P & Boulos M (1993) Mathematical modeling of a freeburning arc in the presence of metal vapor. Journal of Applied Physics 74: 3065–3070.
72. Kramida A, Ralchenko Y, Reader J & NIST ASD Team, (2013) NIST Atomic Spectra Database (version 5.1). National Institute of Standards and Technology, Gaithersburg, MD. Available: <http://physics.nist.gov/asd>. Cited: 3.9.2015.
73. Sanchez JLG, Conejo AN & Ramirez-Argaez MA (202) Effect of Foamy Slag Height on Hot Spots Formation inside the Electric Arc Furnace Based on a Radiation Model. ISIJ International 52(5): 804–713.
74. Peacock GR (2000) Thermal Imaging of Liquid Steel and Slag in a Pouring Stream. Proceedings of SPIE 4020, Thermosense XXII. Orlando. SPIE.
75. Aula M, Fomkin V & Fabritius T (2015) Measurement of Hot-spot Optical Emission Spectrum from Industrial Electric Arc Furnace used in Making of Carbon Steel. Proceedings of the 6th International Congress on Science and Technology of Steelmaking. Beijing, China. The Chinese Society for Metals.

Original publications

- I Aula M, Mäkinen A, Fabritius T (2013) Analysis of arc emission spectra of stainless steel electric arc furnace slag affected by fluctuating arc voltage. *Applied Spectroscopy*. 68(1): 26–32.
- II Aula M, Demus T, Echterhof T, Huttula M, Pfeifer H, Fabritius T (2015) On-line Analysis of Cr₂O₃ content of the slag in pilot scale EAF by measuring the optical emission spectrum of the electric arc. [Manuscript].
- III Aula M, Leppänen A, Roininen J, Heikkinen E.-P, Vallo K, Fabritius T and Huttula M (2014) Characterization of Process Conditions in Industrial Stainless Steelmaking Electric Arc Furnace Using Optical Emission Spectrum Measurements. *Metallurgical and Materials Transactions B*. 45B(6): 839–849.
- IV Aula M, Mäkinen A, Leppänen A, Huttula M, Fabritius T (2015) Optical emission analysis of slag surface conditions and furnace atmosphere during different process stages in electric arc furnace (EAF). *ISIJ International*. 55(8): 1702–170.

Reprinted with permission from Society of Applied spectroscopy (I), Springer (III) and ISIJ International (IV)

Original publications are not included in the electronic version of the dissertation.

542. Ferreira, Eija (2015) Model selection in time series machine learning applications
543. Lamminpää, Kaisa (2015) Formic acid catalysed xylose dehydration into furfural
544. Visanko, Miikka (2015) Functionalized nanocelluloses and their use in barrier and membrane thin films
545. Gilman, Ekaterina (2015) Exploring the use of rule-based reasoning in ubiquitous computing applications
546. Kempainen, Antti (2015) Limiting phenomena related to the use of iron ore pellets in a blast furnace
547. Pääkkönen, Tiina (2015) Improving the energy efficiency of processes : reduction of the crystallization fouling of heat exchangers
548. Ylä-Mella, Jenni (2015) Strengths and challenges in the Finnish waste electrical and electronic equipment recovery system : consumers' perceptions and participation
549. Skön, Jukka-Pekka (2015) Intelligent information processing in building monitoring systems and applications
550. Irannezhad, Masoud (2015) Spatio-temporal climate variability and snow resource changes in Finland
551. Pekkinen, Leena (2015) Information processing view on collaborative risk management practices in project networks
552. Karjalainen, Mikko (2015) Studies on wheat straw pulp fractionation : fractionation tendency of cells in pressure screening, hydrocyclone fractionation and flotation
553. Nelo, Mikko (2015) Inks based on inorganic nanomaterials for printed electronics applications
554. Kursu, Olli-Erkki (2015) Micromotion compensation and a neural recording and stimulation system for electrophysiological measurements
555. Hallman, Lauri (2015) Single photon detection based devices and techniques for pulsed time-of-flight applications
556. Omran, Mamdouh (2015) Microwave dephosphorisation of high phosphorus iron ores of the Aswan region, Egypt : developing a novel process for high phosphorus iron ore utilization
557. Kiljander, Jussi (2016) Semantic interoperability framework for smart spaces

S E R I E S E D I T O R S

A
SCIENTIAE RERUM NATURALIUM

Professor Esa Hohtola

B
HUMANIORA

University Lecturer Santeri Palviainen

C
TECHNICA

Postdoctoral research fellow Sanna Taskila

D
MEDICA

Professor Olli Vuolteenaho

E
SCIENTIAE RERUM SOCIALIUM

University Lecturer Veli-Matti Ulvinen

E
SCRIPTA ACADEMICA

Director Sinikka Eskelinen

G
OECONOMICA

Professor Jari Juga

H
ARCHITECTONICA

University Lecturer Anu Soikkeli

EDITOR IN CHIEF

Professor Olli Vuolteenaho

PUBLICATIONS EDITOR

Publications Editor Kirsti Nurkkala

ISBN 978-952-62-1091-9 (Paperback)

ISBN 978-952-62-1092-6 (PDF)

ISSN 0355-3213 (Print)

ISSN 1796-2226 (Online)

